



Thermal-irradiant performance of green infrastructure typologies: Field measurement study in a subtropical climate city



Wanlu Ouyang^{a,*}, Tobi Eniolu Morakinyo^b, Chao Ren^{c,d}, Sheng Liu^a, Edward Ng^{a,d,e}

^a School of Architecture, The Chinese University of Hong Kong, New Territories, Hong Kong, China

^b School of Geography, University College Dublin, Dublin 4, Ireland

^c Faculty of Architecture, The University of Hong Kong, Hong Kong, China

^d Institute of Future Cities, The Chinese University of Hong Kong, New Territories, Hong Kong, China

^e Institute of Environment, Energy and Sustainability, The Chinese University of Hong Kong, New Territories, Hong Kong, China

HIGHLIGHTS

- Thermal-irradiant behaviors of green infrastructure (GI) were measured and compared.
- Two-way mixed ANOVA found the interactive impacts of time and GI typologies.
- Two typical measurement methods for MRT were used and compared.
- Contributory factors for differences between two MRT measuring methods were examined.
- Implications of GI typologies for sustainable design were discussed.

GRAPHICAL ABSTRACT



ARTICLE INFO

Article history:

Received 14 September 2020

Received in revised form 23 November 2020

Accepted 15 December 2020

Available online 24 December 2020

Editor: Scott Sheridan

Keywords:

Green infrastructure typologies

Field measurement

Thermal-irradiant performance

Mean radiant temperature (MRT)

Outdoor thermal comfort

Subtropical climate

ABSTRACT

Greenery infrastructure (GI) is an important design strategy for sustainable cities and communities' development, as it brings multiple benefits including mitigating urban heat island. Based on the implementation locations, three typical GI typologies, namely green roof, green wall, and ground tree, are widely adopted in urban communities. As previous studies focused on one single GI and mainly studied their thermal features, this study aims to fill the gap by investigating three GI typologies within one site; their thermal-irradiant performance was compared for four typical summer days in a subtropical city. Firstly, stationary and transect measurements were taken for six points (three greenery and three bare points); two typical measuring methods, i.e., the globe thermometer and the six-directional methods, were employed to collect irradiant variables. Secondly, the thermal-irradiant differences were revealed among GI typologies and temporal periods; two measuring methods were compared for their capabilities in detecting the irradiant variations near three GI typologies. Results showed that: 1) the ground tree experienced the smallest thermal-irradiant average and variation among three GI typologies; 2) the morning session (09:00–12:00) had the largest thermal-irradiant reduction and variations for three GI typologies; and 3) the six-directional method showed higher sensitivity towards the irradiant variations near three GI typologies; the globe thermometer method is not suitable for tree-shaded areas. This study provides a comprehensive understanding of proper selection of MRT measuring methods and GI implementation for thermal comfort, especially for the subtropical cities. Practically, this study shows designers and policymakers on how to implement GI typologies for climate-resilient design.

© 2020 Elsevier B.V. All rights reserved.

* Corresponding author.

E-mail address: wanlu.oy@link.cuhk.edu.hk (W. Ouyang).

1. Introduction

1.1. Background of study

According to the projection for 2050, 68% of the global population will live in urban areas, especially in those subtropical and tropical regions given their ongoing rapid urbanization (Ritchie and Roser, 2018). One of the well-known environmental impacts of such urbanization is the urban heat island (UHI) effect, which refers to a higher temperature in urban areas than that in rural areas (Oke et al., 2017). The local UHI effect, together with global climate change, may further exacerbate urban heat risks and worsen the urban residents' health conditions during summertime (IPCC, 2014a). With the intensified UHI effect, most of the less developed countries and regions located in (sub)tropical climate and their citizens could be vulnerable to heat stress. However, in these areas, climate considerations and applications are still lacking in the urban planning and design processes (Roth, 2007). Furthermore, the subtropical climate is predicted to be the main climate type globally in the future given the climate change background (Bastin et al., 2019).

To meet the challenges of changing climate, the corresponding mitigation and adaptation strategies have been investigated, developed, and deployed, especially in (sub)tropical climates (IPCC, 2014b). Among these strategies, the implementation and conservation of urban greenery are favored by governmental officials and urban designers to promote sustainable cities and communities (Ong, 2003), as multiple benefits are brought including combating air and noise pollution, mitigating urban heat island, alleviating psychological stresses, etc. Urban green infrastructure (GI) can be classified into various typologies based on different criteria: property: street trees, private yard greenery, and urban parks (Li et al., 2016); location: ground, vertical, and rooftop greenery (Bartesaghi Koc et al., 2018); species features: deciduous and evergreen (Pérez et al., 2014); different greenery height and planting styles: intensive and extensive green roof, green façade and living walls (Pérez et al., 2014; Nyuk Hien et al., 2007), etc. In this study, GI typologies were defined based on different planting locations, consisted of the ground tree, green wall, and green roof, which is in line with the implementations in the design guidelines (Greening and Development Bureau, 2013; B. Department, 2016).

1.2. Cooling effects of different GI typologies

The cooling capacity of three GI typologies discussed in this study, namely ground tree, green wall, and green roof, have been studied individually in different study areas. Regardless of typologies, cooling was achieved through the processes of shading and evapotranspiration (Gunawardena et al., 2017).

The ground tree has the potential to reduce the solar radiation, cool the ambient temperature, increase the humidity, and improve the outdoor thermal comfort (Lai et al., 2019). Studies in (sub)tropical climate regions found that: in Hong Kong, 0.6 °C air temperature (AT) and 0.1–1.6 °C Physiological Equivalent Temperature (PET) were decreased under the shading of tree canopy (Cheung and Jim, 2018); in Campinas, Brazil, 0.9–2.8 °C and 0.7–2 °C AT was reduced by single trees and tree clusters during 10:00–14:00 h; and 76.2–89.2% of the solar radiation was decreased by different tree species (de Abreu-Harbich et al., 2015); in Malaysia, 73.8–94.7% of the solar radiation was reduced by the canopy (Manoli et al., 2019); in Osaka, Japan, and Tel Aviv, Israel, relative humidity (RH) was increased by 0.5–10.4% and 1.9–7.7% respectively (Yoshida et al., 2015; Shashua-Bar and Hoffman, 2000). These findings indicate that trees have great potential to mitigate the UHI effect and improve outdoor thermal comfort.

The green wall is another promising measure to counterbalance the urban heat island effects (Alexandri and Jones, 2008), as it modified microclimate through shadow, evapotranspiration, and thermal insulation (Perez et al., 2011). In Singapore, 12.8 °C mean radiant temperature

(MRT) and 1.3 °C AT were reduced near the green wall (Liang et al., 2014). Another study in Singapore measured up to 3.33 °C AT reduction by green wall (Wong et al., 2010). In Chicago, the USA, areas near the vertical greenery had 0.8–2.1 °C lower AT and less fluctuated RH compared with the bare façades (Susorova et al., 2014). In Nanjing, China, the mean surface temperature reduction was 2.6 °C (Yin et al., 2017), this value was 4.0–12.0 °C in Singapore (Wong et al., 2010) and 12.0–20.0 °C in Italy (Mazzali et al., 2013). Outgoing heat fluxes were reduced 23.0–37.0 W/m² by the green wall in Italy (Mazzali et al., 2013). All of the above observations were made less than 1.5 m distance from the walls, which indicates vertical greenery adjacent to pedestrian footpaths may effectively improve the outdoor thermal comfort (Middel and Krayenhoff, 2019).

The green roof was mostly discussed for energy saving through shading, thermal insulation, and evapotranspiration (Raji et al., 2015). Recently, the heat island mitigation potential of green roofs has been explored (Santamouris, 2014). In Singapore, the surface temperature was reduced up to 30 °C, and AT was decreased up to 4.2 °C within a limited height by the green roof; 109 W/m² solar radiation was decreased at noontime (Wong et al., 2003). In Hong Kong, cooling provision by green roof was averagely 1.7–4.9 °C in surface temperature, 0.6–1.6 °C in AT, 4.5–10.9 °C in PET, 2.3–5.5 °C in Universal Thermal Climate Index (UTCI) (Lee and Jim, 2019). In Melbourne, an irrigated green roof can provide a substantial microclimate benefit during the day, as AT was reduced by decreasing sensible heat (Coumts et al., 2013). In Netherland, a slightly warming effect was observed for a green roof during the day, and the same study also emphasized further research is needed for the impact of the green roof towards AT (Solcerova et al., 2017). In the meantime, some studies found green roofs can attenuate urban heat at the city scale (Krayenhoff et al., 2018; Yang and Bou-Zeid, 2019). Moreover, some researchers noted the unbalanced distribution of modeling studies vs. measurement studies, and the majority of the evidence of green roof was model-based (Francis and Jensen, 2017; D'Orazio et al., 2012; Ouldboukhitine et al., 2014).

Based on the discussions above, it is clear that the cooling intensity varies with different urban greenery typologies. These variations are caused by several potential factors, such as local climate, urban morphological conditions, spatial scales, temporal periods, (micro)-meteorological parameters, and the specific GI typologies, etc. (Gunawardena et al., 2017), which limit cross-comparisons due to the uncertainties arising from non-identical contexts. However, limited studies measured the thermal-irradiant features (thermal and irradiant variables) of GI typologies within one study site, which hinders the comparability of GI thermal-irradiant performances (Bartesaghi Koc et al., 2018). Furthermore, solar radiation fluctuates along with time so that the thermal-irradiant performances of greenery should be varied. However, temporal fluctuations in the thermal-irradiance have seldom been compared for GI typologies in previous studies. A detailed understanding of the temporal variations of GI cooling performance is also an essential step in developing climate responsive design strategies accordingly.

1.3. Mean radiant temperature and its measuring methods

Mean radiation temperature (MRT) is defined as the “uniform temperature of an imaginary enclosure in which the radiant heat transfer from the human body equals the radiant heat transfer in the actual non-uniform enclosure” (ASHRAE, 2001). With its dependence on incoming shortwave radiation during daytime, MRT is mostly impacted by shading effects of greenery, as the foliage impede the direct solar radiation so that the shortwave radiation and MRT are decreased underneath the foliage or canopy (Cheung and Jim, 2018). Besides, surface temperature can be reduced by shading, then longwave radiation of lateral directions is decreased as well (Middel and Krayenhoff, 2019). Comparing with other parameters, MRT not only captures thermal variations at a fine-scale, but also involves in the calculation of thermal indices, i.e., Physiological Equivalent Temperature (PET), and Universal Thermal Climate Index

(UTCI) (Thorsson et al., 2007; Lai et al., 2017). Given the highly spatial variations in thermal exposure, MRT is widely used in outdoor thermal comfort studies to explain the thermal responses of a human being towards his surrounding environment (Tan et al., 2013).

There are two main methods to measure MRT in the outdoor environment: the globe thermometer and the six-directional method (Kántor et al., 2015). The global thermometer method is based on the radiation and convective heat exchange processes between the globe thermometer and the environment (Kántor et al., 2015). This method is convenient and cheap, yet with shortcomings including longer equilibrium time, non-representative for radiation load of a human, and overestimation in short-wave radiation compared to a human body (Toudert, 2005; Heating, A.S.o., Refrigerating, and A.-C. Engineers, 1985). The six-directional method sums up short- and long-wave flux in six directions (i.e., four lateral, upper, and down) (Kántor et al., 2015), which has higher accuracy and can measure heat fluxes in different directions (Tan et al., 2013). Previous studies compared the accuracy between these two methods, which mainly focused on areas with limited greenery, such as the squares and courtyard (Thorsson et al., 2007; Thorsson et al., 2006), streets with nearly no greenery (Krüger et al., 2014), and pedestrian sidewalks (Khrit et al., 2017). However, rare studies compared these two methods affected by greenery, especially for different GI typologies. As MRT is also largely affected by greenery shading during the daytime (Tan et al., 2016), the comparison between two methods is necessary for different GI typologies.

1.4. Objectives

Given the knowledge gap mentioned above, this study aims to: 1) measure the thermal-irradiant performance of GI typologies within one site to control the background environmental setting and ensure the cross-comparisons; 2) compare the thermal-irradiant differences among three GI typologies and three temporal periods in daytime; and 3) compare the sensitivity of two MRT measuring methods towards three GI typologies. The sensitivity here refers to the capacity of detecting the ranges and variations in the irradiant features in the built environment with different GI typologies. The results of this study can serve as a reference to other (sub)tropical areas in understanding the thermal-irradiant

behaviors of different GI typologies, and furtherly assist scientific recommendations on greenery design and implementations at a community scale, especially for the priorities and distributions of different GI typologies.

2. Materials and methods

2.1. Study area and measurement site

Hong Kong (HK), with a hot-humid subtropical climate (Cfa based on Köppen climate classification), is taking a leading role in taking actions to combat climate change and providing insights for other (sub) tropical cities (Ren et al., 2011). According to the records revealed by Hong Kong Observatory (HKO), the summer period in HK ranges from June to September, with 28.5 °C temperature and 80% relative humidity in daily average (Chen et al., 2012). A changing trend of weather conditions has been observed according to historical temperature records; 2019 was the warmest year since 1884 with an annual average of 24.5 °C, 1.2 °C higher than the normal of 1981–2010 (Hong Kong Observatory, 2020a). The temperature is predicted to continuously rise by 1–2 °C and 1.5–3 °C in the mid- and late 21st century, compared to the average of 1986–2005 (Hong Kong Observatory, 2020b).

The government of HK has taken various efforts to engage the key private-sector stakeholders and the public in combating climate change. Usually, government buildings set examples to the public for sustainability establishment. Therefore, the measurement site in this study located in the courtyard of the Electrical and Mechanical Services Department (EMSD) of the Hong Kong Government. EMSD is situated in the Kowloon area, with the most populous urban area in Hong Kong (Fig. 1). Within this site, three GI typologies are present and close in proximity; the volume of pedestrian and transportation is small so that the impacts of anthropogenic heat on measurement results are minimal.

2.2. Instruments and measurement campaign

2.2.1. Instruments setting-ups and recalibration

Measurements were conducted using HOBO U12 Data loggers, TESTO480, CNR4 Net Radiometer (with LogBox SE), and LI-COR

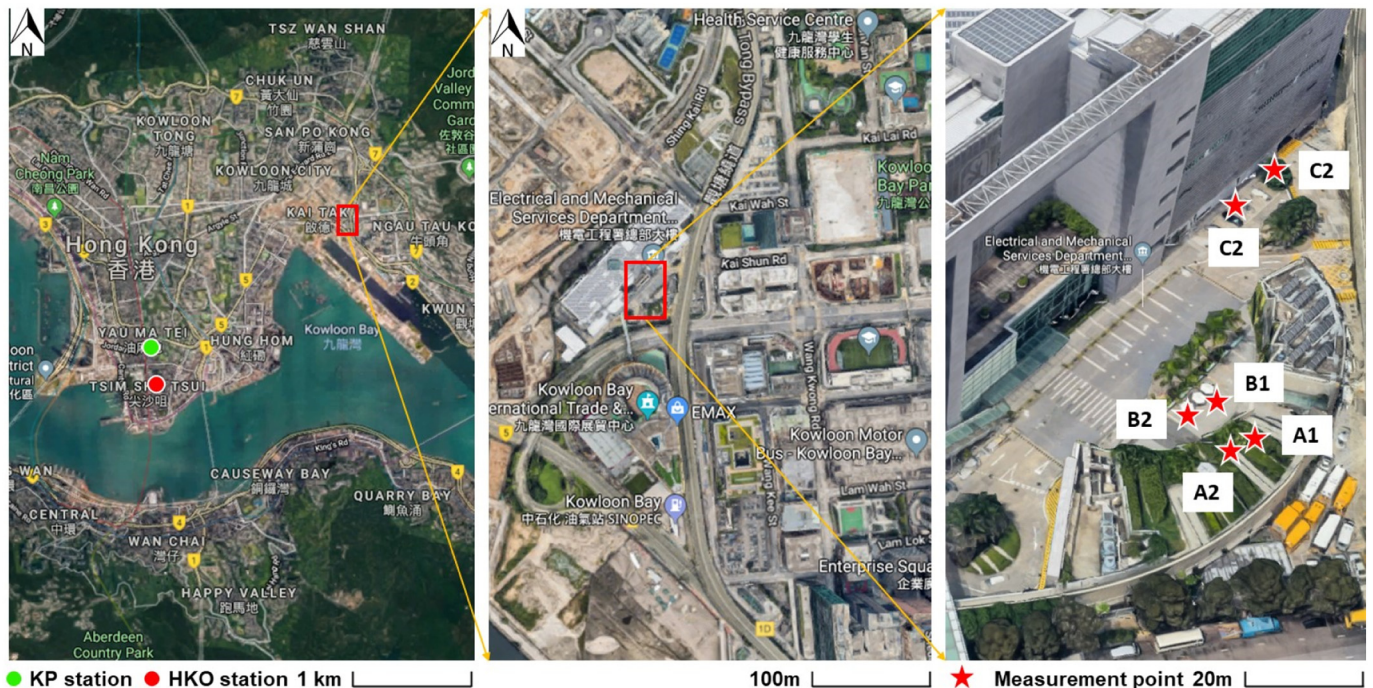


Fig. 1. Case study site (source: Google map).



* According to standard EN 60584-2, the accuracy of Class 1
Not mentioned in the product manual and application information

Sensor	Variable(s)	Range	Accuracy	Response Time	Sampling Time
1 HOBO U12-012	Air temperature Relative humidity	-20°C to +70°C 5% to 95%	± 0.3 °C + 2.5 %	AT: 6min RH: 1min	10s
2 LI-200SA Pyranometer	Global solar radiation	0.4-0.95 μm for spectral response	Typically 80 μA per 1000 Wm ⁻²	10 μs	5s
3 TESTO 480 Comfort level probe	Wind speed Wind direction	0 to 5 m/s	±(0.03 m/s + 4 % of mv)	/ #	5s
4 TESTO 480 Temperature probe	Air temperature Relative humidity	-20 to +70 °C 0 to 100 %RH	±0.2 °C ±1% RH	/ #	5s
5 TESTO 480 Global thermometer 40mm	Global temperature	0 to 120 °C	±x 0.004 *	<5min	5s
6 CNR4 Component net radiometers	Shortwave and Longwave radiation	0.3 to 2.8 μm 4.5 to 42 μm	5 to 20 μV/W/m ²	< 18 s	5s

Fig. 2. Measurement instruments setup (left); sensor specifications (right).

pyranometer (LI-200SA and LI-1400 data logger), which were widely used in previous studies (Cheung and Jim, 2018; Middel and Krayenhoff, 2019; Morakinyo et al., 2017). The setup, parameter measured by each instrument, and sensors' specifications can be found in Fig. 2. It should be mentioned that our study used the 40 mm globe thermometer instead of a 150 mm diameter copper sphere. On one hand, smaller diameter size in globe thermometer was widely used in the outdoor studies for microclimate (Cheung and Jim, 2018; Liang et al., 2014; Tan et al., 2013; Thorsson et al., 2006). On the other hand, the equilibrium time was affected by the sphere diameter and a smaller sphere will shorten the response time, less than 5 min (Thorsson et al., 2007; Kántor et al., 2015).

During the measurement, all devices were set at the pedestrian level (1.5 m height for all GI typologies, and 1 m distance from the green wall). Before the field measurement in September 2019, sensors recalibration tests were conducted on the roof of a building in the Chinese University of Hong Kong (see Supplementary file S1).

2.2.2. Measurement campaign: spots and procedure

Six monitoring spots were set for the measurement, two (reference and greenery points) for each GI typology (see Fig. 1). As shown in Fig. 3, A1 and A2 represent green roof and bare roof location; B1 and B2 represent green wall and bare wall location; C1 and C2 represent tree-shaded grass covering and tree-free concrete pavement location. Each pair are within 3 m distance; thus, the surrounding environment was similar and with minimal biases between paired locations.

The measurement campaign includes two parts: stationary monitoring and transect measurements. For each monitoring point, a HOBO U12 Data Logger was set for stationary monitoring, while the TESTO480, LICOR, and CNR4 Net Radiometer were coupled for transect measurement. The transect procedure included 8 rounds and each round was within 1 h as shown in Fig. 4. During each round, the transect measurement started at A1 and ended at C2. For each monitoring point, the measurement lasted for 5 min, then the transect instruments were shifted to the next point and were allowed to stabilize, which would take another 5 min. For each shifting, at least 2 min is ensured for the sensor's response and stabilization time. This kind of setting was supported by the conclusion in the previous studies that a 40 mm globe thermometer shortens the response time within 5 min (Thorsson et al., 2007; Kántor et al., 2015). To further justify the stabilization of the 40 mm globe was achieved in our study, ANOVA was taken between the values of the 5 min, and last 4, 3, 2, and 1 min, and the results showed there was no significant difference between them (see Supplementary file S2). Therefore, this study assumed the 40 mm globe thermometer has been stabilized during the 5 min measurement and the values during the 5 min were used in the following analysis.

The measurement started at 09:30 h and ended at 17:25 h on each of four days: September 07th, 09th, 11th, and 12th, 2019, with typical summer weather conditions in Hong Kong as partially cloudy (Tan et al., 2017). All devices were synchronized every day before starting the measurement. The detailed weather conditions were summarized in Table 1, according to the weather records of two representative stations with long-term service time: HKO (Hong Kong Observatory) station and KP (King's park) station (locations were shown in Fig. 1).

2.3. Methods of data analysis

2.3.1. Calculation of mean radiant temperature (MRT)

Two typical and widely measuring methods for MRT were employed in this study. The globe thermometer has advantages in the low-costs and convenient application therefore is still widely used in recent microclimate and greenery studies (Cheung and Jim, 2018; Liang et al., 2014; Lee and Jim, 2019). The six-directional method is more accurate but requires higher in equipment settings. Understanding the correlations and differences between these two methods is important, especially for different urban geometry contexts with different GI typologies.

2.4. The globe thermometer method

The globe thermometer method rests on the assumption that an equilibrium state is achieved in the globe between gained and lost heat through radiation and convection processes so that the globe temperature reflects both radiant and ambient temperature (Kuehn et al., 1970). By measuring globe temperature, air temperature, and wind velocity, MRT can be calculated with Eq. (1) (Thorsson et al., 2007):

$$MRT = \sqrt[4]{(T_g + 273.15)^4 + \frac{1.1 \times 10^8 \cdot V_a^{0.6}}{\epsilon \cdot D^{0.4}} \cdot (T_g - T_a)} - 273.15 \quad (1)$$

where T_g is the temperature measured by the globe [°C], V_a is the wind speed [m/s], T_a is the air temperature [°C], D is the globe diameter (= 40 mm), ϵ is the globe emissivity (= 0.95).

2.5. The six-directional method

The six-directional method assumes the human body as a cube, thus MRT can be calculated by the weighted sum of all long- and short-wave radiant fluxes (Chen et al., 2014). By measuring the radiant flux at the six directions, MRT can be calculated based on Eqs. (2)–(5) (Lai et al., 2017).

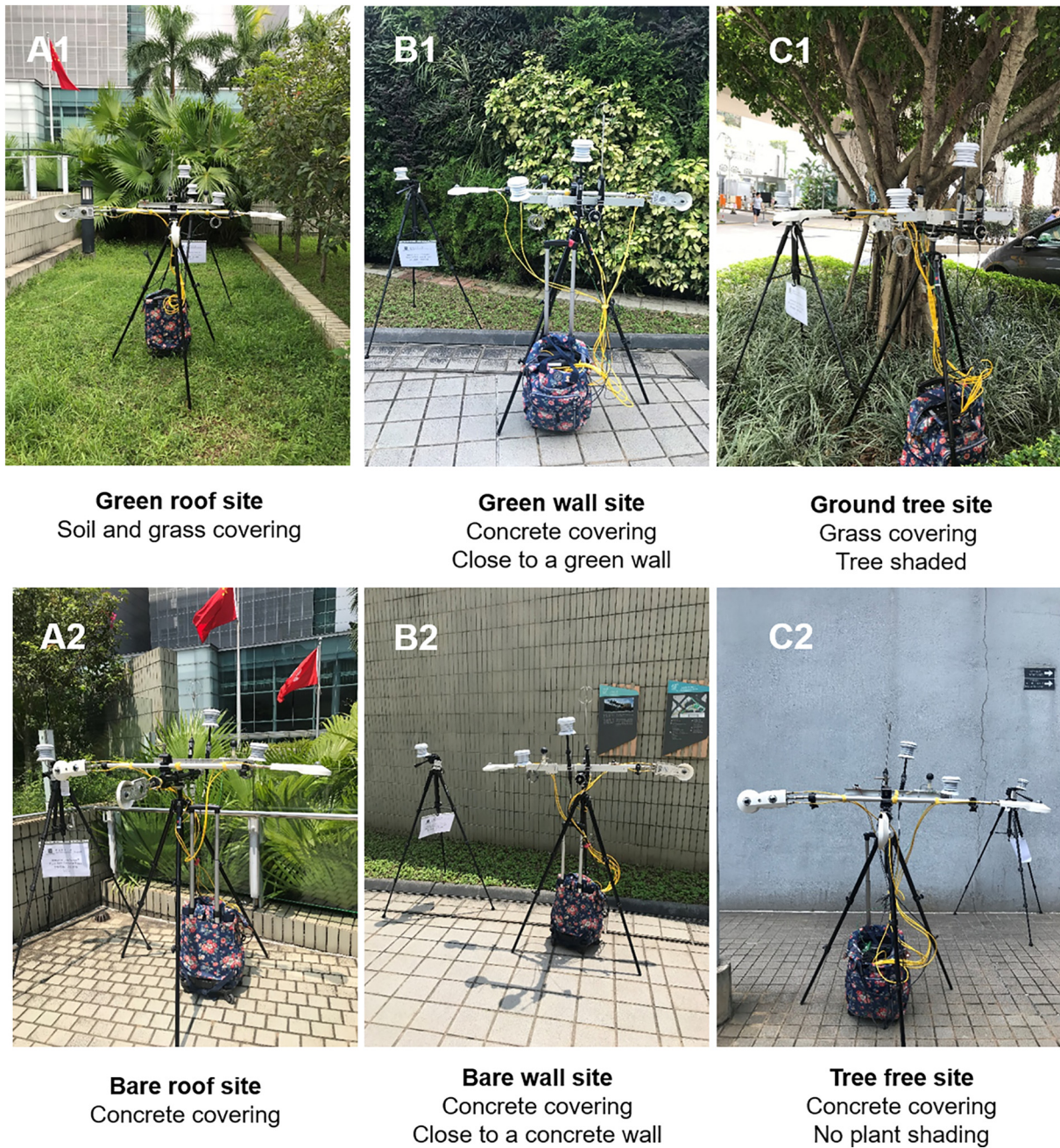


Fig. 3. Six measurement points and surrounding environments in the study.

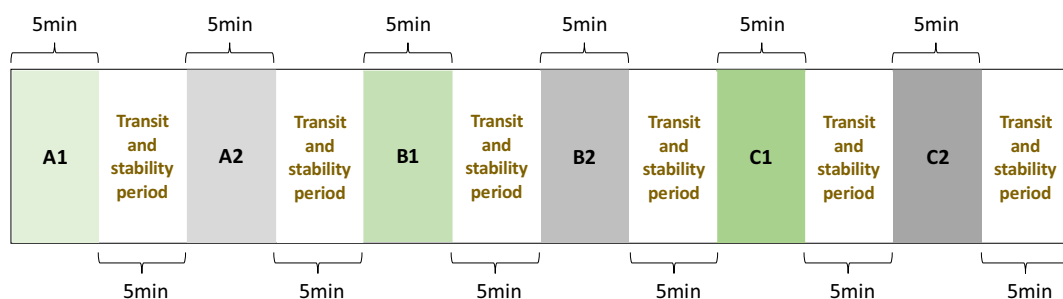


Fig. 4. Transect measurement procedure of one round (within 1 h).

Table 1
The weather features in four survey days (9:00–18:00 h).

Date (YYYY-MM-DD)	Air temperature (°C)*			Relative humidity (%)*			Wind conditions†	
	Min.	Max.	Mean	Min.	Max.	Mean	Mean speed (m/s)	Mode direction (°)
2019-09-07	29.0	33.0	31.36	65.0	83.5	71.0	1.57	255
2019-09-09	29.8	33.0	31.25	65.0	77.5	71.8	1.99	265
2019-09-11	29.1	32.9	31.64	60.0	77.0	66.4	2.56	113
2019-09-12	29.7	33.4	31.73	61.0	75.0	67.2	2.76	90

Note: HKO (since 1884) and KP (since the 1950s) are two representative stations with long-term services.

* From the HKO station.

† From the KP station (shown in Fig. 1).

$$WSumL = \epsilon_p \sum_{i=1}^6 W_i * L_i \tag{2}$$

$$WSumK = a_k \sum_{i=1}^6 W_i * K_i \tag{3}$$

$$S_{Str} = WSumL + WSumK \tag{4}$$

$$MRT = \sqrt[4]{S_{Str} / (\epsilon_p * \sigma)} - 273.15 \tag{5}$$

where L_i and K_i are longwave and shortwave fluxes from i th direction; a_k and ϵ_p are the absorption coefficients of the clothed human body for short- and long-wave radiation ($=0.7$ and 0.97 respectively); σ is Stefan-Boltzmann constant ($=5.67 * 10^{-8} \text{W/m}^2 \text{K}^4$), and W_i is an angular factor for six different directions with the sum weightings equals 1 ($=0.22$ for the lateral, 0.06 for the up-down directions).

Besides, two components of radiant fluxes were calculated. Firstly, the sum of longwave radiant fluxes was calculated based on weightings in six directions in Eq. (2). Based on this, longwave radiant temperature (LMRT) was calculated by replacing S_{Str} with $WSumL$ in Eq. (5), which represents the effective longwave fluxes emitted and reflected from the surrounding. After that, the differences between MRT and LMRT (MRT-LMRT) were extracted to represent the effective shortwave irradiance reflected by the surrounding and scattered by the sky (Lai et al., 2017).

2.5.1. Statistical analysis

Descriptive statistics was firstly conducted to describe the distribution of the data. Then two kinds of analysis of variance (ANOVA) were used to compare the differences between samples. To compare the

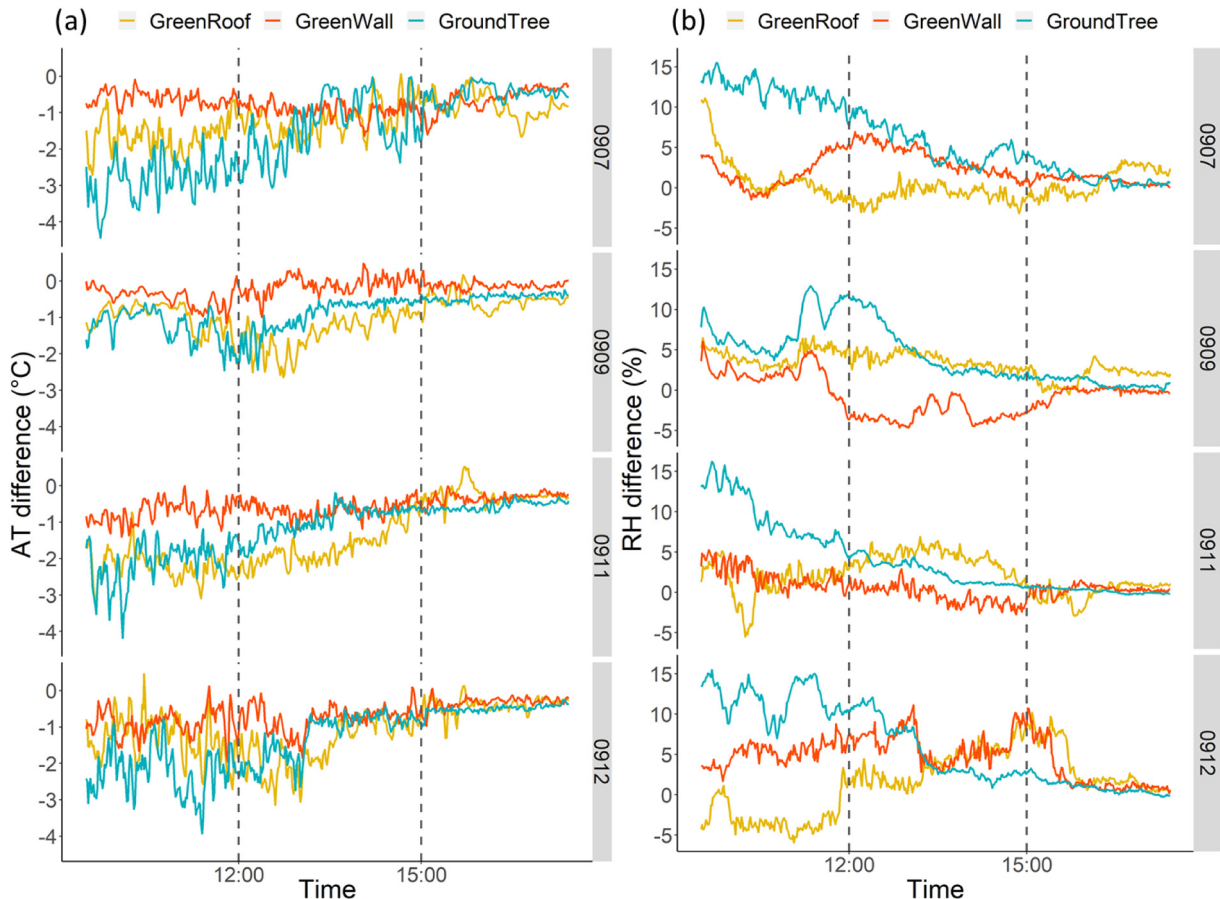


Fig. 5. (a) Air temperature (AT) and (b) relative humidity (RH) differences in four measurement days (YYYY-MM-DD: 2019-09-07, 09/09/2019, 11/09/2019, 12/09/2019) by HOBO (9:30–17:25) (dash line represents the division of three periods).

thermal and irradiant differences between GI typologies, one-way ANOVA was employed. Whether ANOVA showed a significant difference or not, a post hoc analysis was applied to identify where the differences were located. Afterwards, a two-way mixed ANOVA was applied to examine the main effects of different temporal periods, GI typologies, and their interaction (temporal periods \times GI typologies) over the variations in AT, RH, and radiant features. GI typologies acted as a between-subjects factor, whereas time was the within-subjects factor. Then post hoc analysis was applied for multiple comparisons to detect the factors that account for the differences. When an interactive effect was found by ANOVA, Tukey's test was applied to examine the different combinations of GI typologies and periods. Meanwhile, correlation tests were conducted between MRT values measured by the two methods; associations between MRT by two methods and potential factors to explain the differences, i.e., wind speed, solar radiation, and radiant fluxes components, were also analyzed. All of these analyses were conducted in R (version 3.6.3) (R Core Team, 2020).

3. Results

3.1. Comparing thermal behaviors of three GI typologies

3.1.1. Thermal differences observed by stationary instruments

Fig. 5 shows the differences in air temperature (AT) and relative humidity (RH) between the greenery and bare counterparts of the three GI typologies, which was measured by the stationary HOBO stations between 9:30 and 17:25 on the four measurement days. In terms of AT difference, the green wall presented no more than 1 °C cooling and fewer variations across the temporal periods. The green roof had moderate fluctuations with higher AT difference in the morning and lower values in the afternoon. The ground tree had similar trends with the green roof

but had the highest AT difference before noon with up to 4 °C, and less than 1 °C in the afternoon. This variation in different periods can be explained partly by the changing solar path and radiation. As for RH difference, the ground tree always increased moisture during the monitoring periods, while the green wall and the green roof sometimes decreased RH slightly, especially during noon. The highest RH difference was detected as 16% under the ground tree in the morning. The details of descriptive statistics were summarized in Table A1 in the Appendix. Given the AT and RH were significantly affected by temporal periods, thus in the following analysis, three temporal periods were divided and considered: morning (9:30–12:00), noon (12:01–15:00), and afternoon (15:01–17:25).

3.1.2. ANOVA analysis in the thermal difference

One-way ANOVA was conducted to test the thermal difference of GI typologies, and two-way mixed ANOVA was adopted to measure the effect of temporal periods and GI typologies, as well as their interactive impacts. The ANOVA results for AT and RH were shown in Fig. 6.

For the AT difference, the mean \pm sd of green roof (-1.19 ± 0.70 °C) and ground tree (-1.24 ± 0.87 °C) presented higher values and variations than that of the green wall (-0.54 ± 0.36 °C). Shown in Fig. 6(a), one-way ANOVA results indicated significant difference among three GI typologies, with $F(2, 5709) = 624, p < 0.0001$. A post-hoc multiple comparison test showed significant differences between each pair of GI typologies: green wall vs. green roof ($p < 0.0001$), ground tree vs. green roof ($p < 0.05$), and ground tree vs. green wall ($p < 0.0001$). The two-way mixed ANOVA shown in Fig. 6(b) revealed both significant main effects of temporal periods and GI typologies with $F(2, 5703) = 1803.9, p < 0.0001, \eta^2 = 0.279$ and $F(2, 5703) = 1161.2, p < 0.0001, \eta^2 = 0.179$ respectively. There was also a significant interaction of temporal periods and GI typologies, with $F(2,$

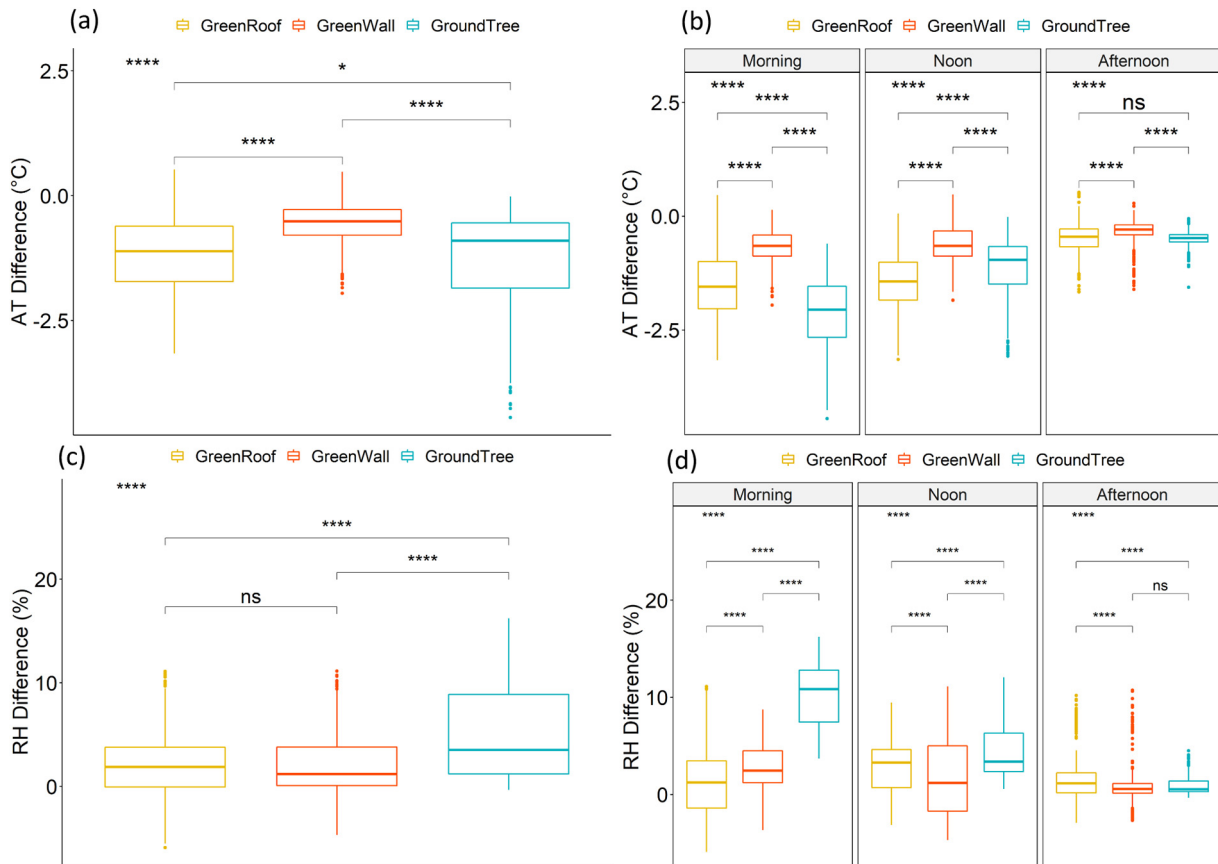


Fig. 6. One-way and two-way ANOVA analysis results (a, b) for AT and (c, d) for RH (significance code: ns – $p > 0.05$; * – $p \leq 0.05$; ** – $p \leq 0.01$; *** – $p \leq 0.001$; **** – $p \leq 0.0001$).

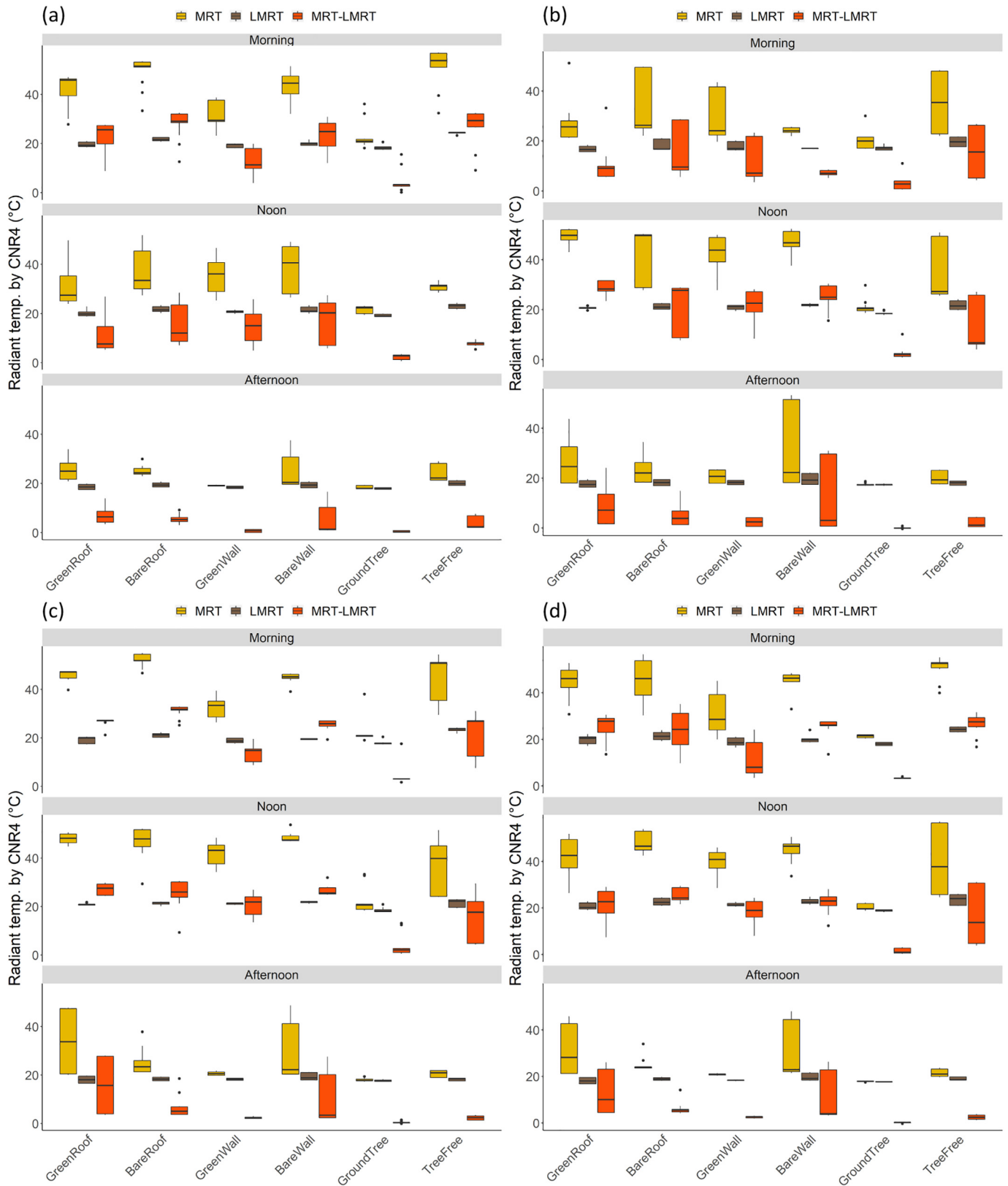


Fig. 7. MRT and irradiant elements (LMRT, MRT-LMRT) during three periods in four measurement days: (a) 0907, (b) 0909, (c) 0911 and (d) 0912.

5703) = 328.4, $p < 0.0001$, $\eta^2 = 0.101$. Furthermore, the post-hoc multiple comparison test showed that there was no significant difference between green roof vs. ground tree in the afternoon ($p > 0.05$), but

statistically significant AT differences were found between each pair of GI typologies in the morning and noon periods, and two remaining pairs in the afternoon.

Regarding the RH difference, ground tree ($5.20 \pm 4.55\%$) exhibited higher values and variation than green roof ($1.82 \pm 2.83\%$) and the green wall ($1.74 \pm 2.95\%$). The results of one-way ANOVA showed that a significant difference existed between the humidity impact of GI typologies with $F(2, 5709) = 598.2, p < 0.0001$ (see Fig. 6(c)). A post-hoc test indicated that there was no significant difference between moisture contents near the green roof and green wall ($p > 0.05$) whereas significant differences were found between green roof vs. ground tree ($p < 0.0001$), as well as green wall vs. ground tree ($p < 0.0001$). A two-way ANOVA showed that there was a significant main effect of temporal period ($F(2, 5703) = 805.1, p < 0.0001, \eta^2 = 0.138$), and a significant main effect of greenery type ($F(2, 5703) = 1008.7, p < 0.0001, \eta^2 = 0.173$). Also a significant interaction of period and greenery type was found with $F(2, 5703) = 578.4, p < 0.0001, \eta^2 = 0.199$ (Fig. 6(d)). The post-hoc multiple comparison test showed that although there was a significant difference between each pair of GI typologies in both morning and noon period, and the RH differences were also significant between ground tree vs. green roof ($p < 0.0001$), ground tree vs. green roof ($p < 0.0001$) in the afternoon, but not for green wall vs. ground tree during the afternoon ($p > 0.05$).

3.2. Comparing irradiant behaviors of three GI typologies

As the irradiant values of greenery and bare spots were not collected simultaneously, in this section, six points were analyzed separately instead of calculating greenery-bare differences. Besides, this section mainly focused on irradiant values measured by CNR4, including MRT, LMRT, and MRT-LMRT.

3.2.1. Irradiant features measured by transect measurement

Fig. 7 showed the radiant temperature distribution during three periods in the four measurement days respectively, including mean

radiant temperature (MRT) and its irradiant elements (LMRT, MRT-LMRT) at the six monitoring points. Overall, GI points had lower mean values and fewer fluctuations than bare counterpart points. The highest mean MRT value was observed at the bare roof location ($39.57 \pm 12.26\text{ }^\circ\text{C}$), followed by the green roof ($38.36 \pm 11.17\text{ }^\circ\text{C}$), the bare wall ($37.36 \pm 11.93\text{ }^\circ\text{C}$), the tree-free ($32.78 \pm 12.93\text{ }^\circ\text{C}$), the green wall ($31.83 \pm 9.70\text{ }^\circ\text{C}$), and the ground tree ($20.08 \pm 3.32\text{ }^\circ\text{C}$). The detailed results of the descriptive statistics of radiant temperature within four days can be found in Table A2 in the Appendix. MRT values were mainly affected by MRT-LMRT which represents the effective sum of shortwave radiations received from the surroundings and the sky (Lai et al., 2017). LMRT primarily fluctuated around $20\text{ }^\circ\text{C}$ and had smaller ranges than MRT and MRT-LMRT. Regarding temporal periods, morning and noon sessions experienced higher radiant temperatures than that of the afternoon, which was caused by weather conditions during the day that the weather turned from sunny to partially cloudy and finally cloudy. Besides, due to the changing solar path, the EMSD building provided shading for the site in the afternoon.

To further understand the different contributions of irradiant features in MRT values, the proportions of LMRT and MRT-LMRT to MRT were calculated and shown in Fig. 8. For the diurnal periods, in the tree point, LMRT constituted a high proportion of MRT above 80%, which indicated the shading effects of the tree canopy. Other points in open areas, such as the roof-pair and the bare wall points, MRT-LMRT made up over 50% contributions, which means solar radiation affected a lot. For different temporal periods, due to the changing weather conditions from sunny to partially cloudy, MRT-LMRT dominated in the morning and LMRT dominated in the afternoon session. In the noontime, the percentages of LMRT and MRT-LMRT were in the equal distribution for all points except the ground tree spot.

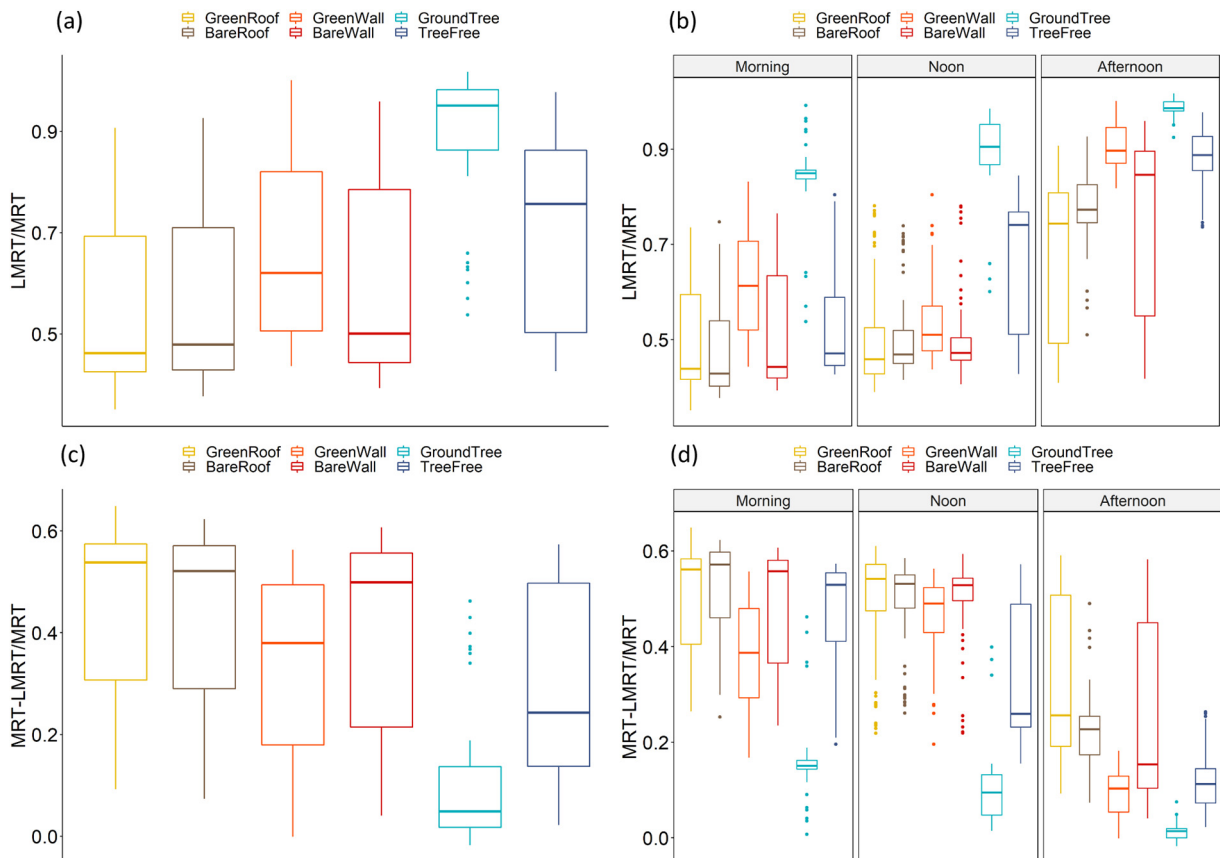


Fig. 8. Percentage of irradiant elements to MRT: (a, b) for LMRT and (c, d) for MRT-LMRT.

3.2.2. ANOVA analysis in irradiant difference

Similar to Section 3.1.2, one-way and two-way ANOVA analyses were conducted for radiant temperature from the six monitoring points. Fig. 9 showed the ANOVA results for radiant temperature in daytime and three temporal periods. For MRT, significant differences were observed among six points with $F(5, 954) = 71.96, p < 0.0001$. However, a further post-hoc test revealed no significant difference between the green roof and the bare roof ($p > 0.05$) while other pairs showed significant differences at $p < 0.0001$ level (see Fig. 9(a)). Two-way mixed ANOVA was employed to understand the effects of GI typologies and temporal period on MRT variation. Shown in Fig. 9(b), a significant effect was found for the temporal periods ($F(2, 942) = 14.969, p < 0.0001, \eta^2 = 0.022$), and GI typologies ($F(5, 942) = 75.742, p < 0.0001, \eta^2 = 0.274$). The interactive effect of GI typologies

and temporal periods was also found to be significant with $F(10, 942) = 3.221, p < 0.0001, \eta^2 = 0.023$. The post-hoc tests revealed significant differences between each pair during the morning and the afternoon. As for the noon period, green roof vs. bare roof and green roof vs. green wall pairs showed no significant differences ($p > 0.05$). As for LMRT, significant differences were observed among six points with $F(5, 954) = 58.24, p < 0.0001$. No significant difference between the green roof and green wall ($p > 0.05$) while other pairs showed significant differences at $p < 0.0001$ level (see Fig. 9(c)). Two ANOVA results showed a significant effect for the temporal period of the day ($F(2, 942) = 1076.6, p < 0.0001, \eta^2 = 0.266$), and GI typologies ($F(5, 942) = 108.88, p < 0.0001, \eta^2 = 0.234$), as well as an interactive effect on LMRT caused by GI typologies and temporal periods with $F(10, 942) = 22.17, p < 0.0001, \eta^2 = 0.095$ (see Fig. 9(d)). But no differences

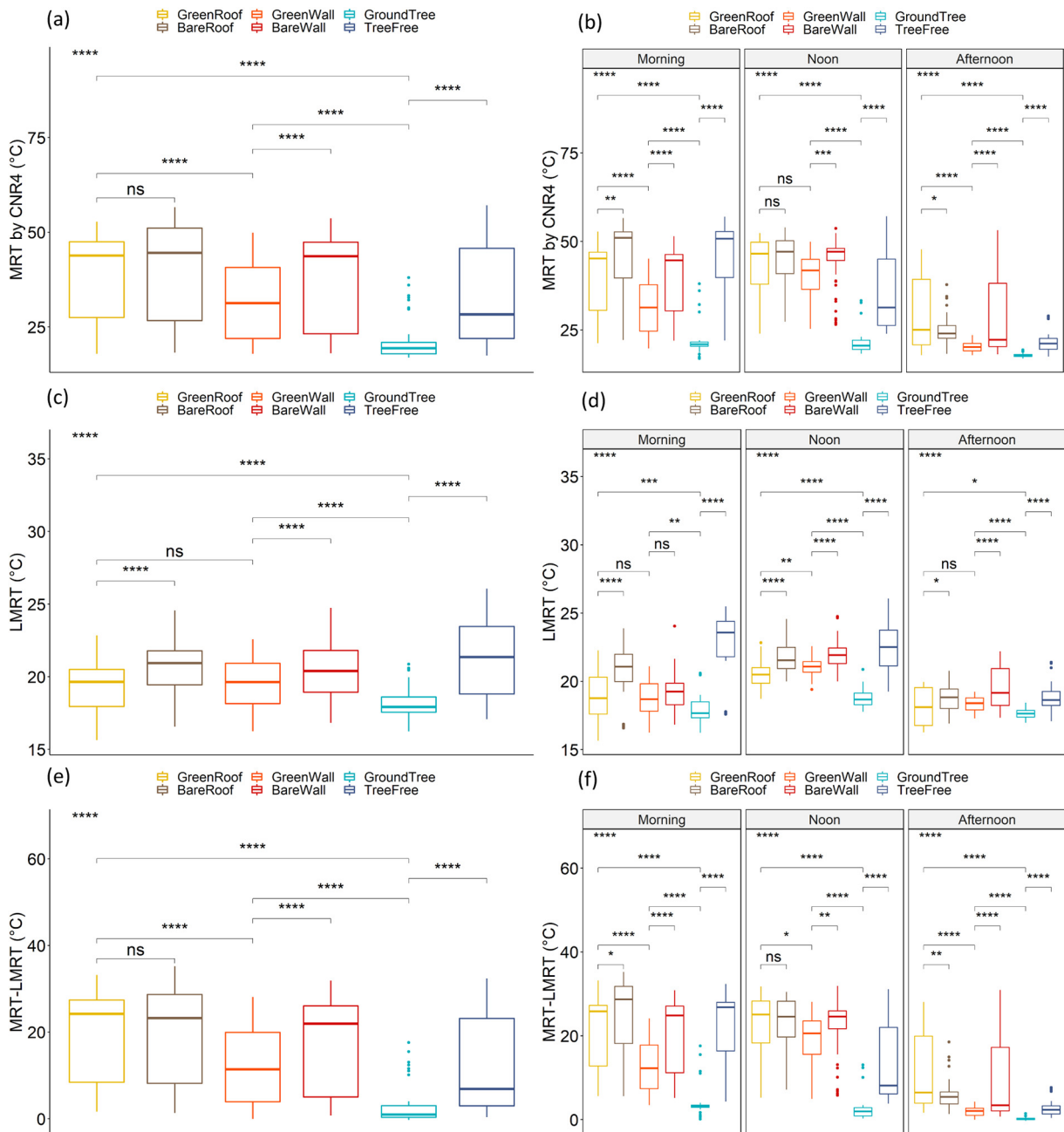


Fig. 9. ANOVA analysis results for radiant temperature by CNR4 in daytime and three periods (a, b) for MRT; (c, d) for LMRT; (e, f) for MRT-LMRT (significance code: ns – $p > 0.05$; * – $p \leq 0.05$; ** – $p \leq 0.01$; *** – $p \leq 0.001$; **** – $p \leq 0.0001$).

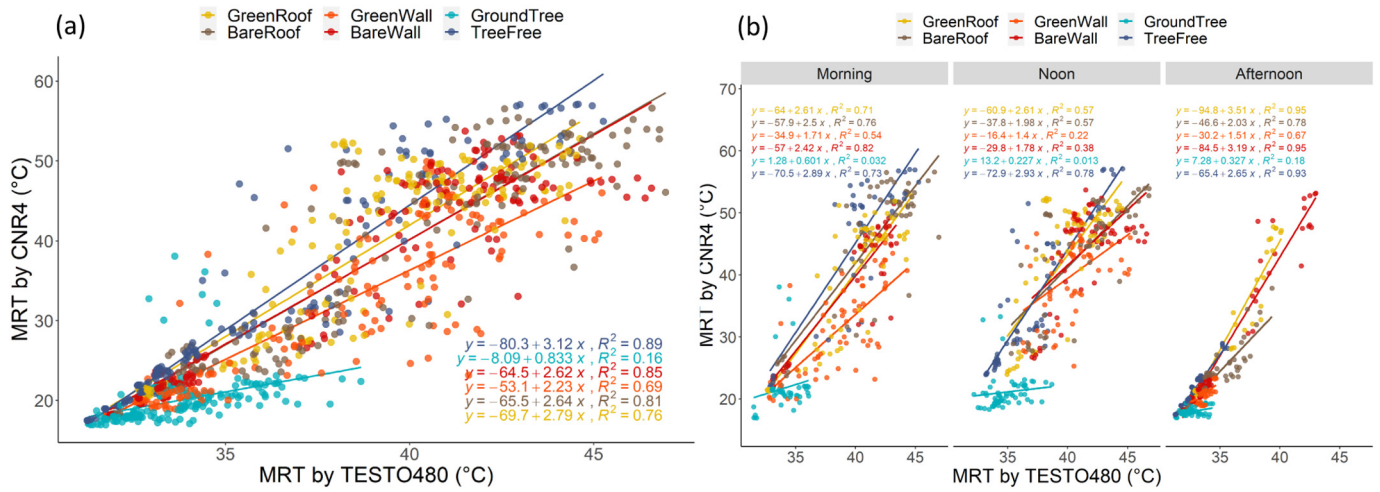


Fig. 10. Correlation between the MRT measured by two methods (a) daytime, (b) three temporal periods.

were observed for green roof vs. green wall in the morning and afternoon, and green wall vs. bare wall in the morning. Regarding MRT-LMRT, one-way ANOVA both showed significant results with $F(5, 954) = 77.95, p < 0.0001$, but post-hoc tests showed no significant difference for green roof vs. bare roof ($p > 0.05$). Two-way ANOVA showed a significant effect for the temporal period of the day ($F(2,$

$942) = 264.97, p < 0.0001, \eta^2 = 0.231$), and GI typologies ($F(5, 942) = 133.25, p < 0.0001, \eta^2 = 0.290$), as well as an interactive effect on LMRT caused by GI typologies and temporal periods with $F(10, 942) = 15.89, p < 0.0001, \eta^2 = 0.069$. But no difference was found between the green roof and the bare roof at the noontime ($p > 0.05$).

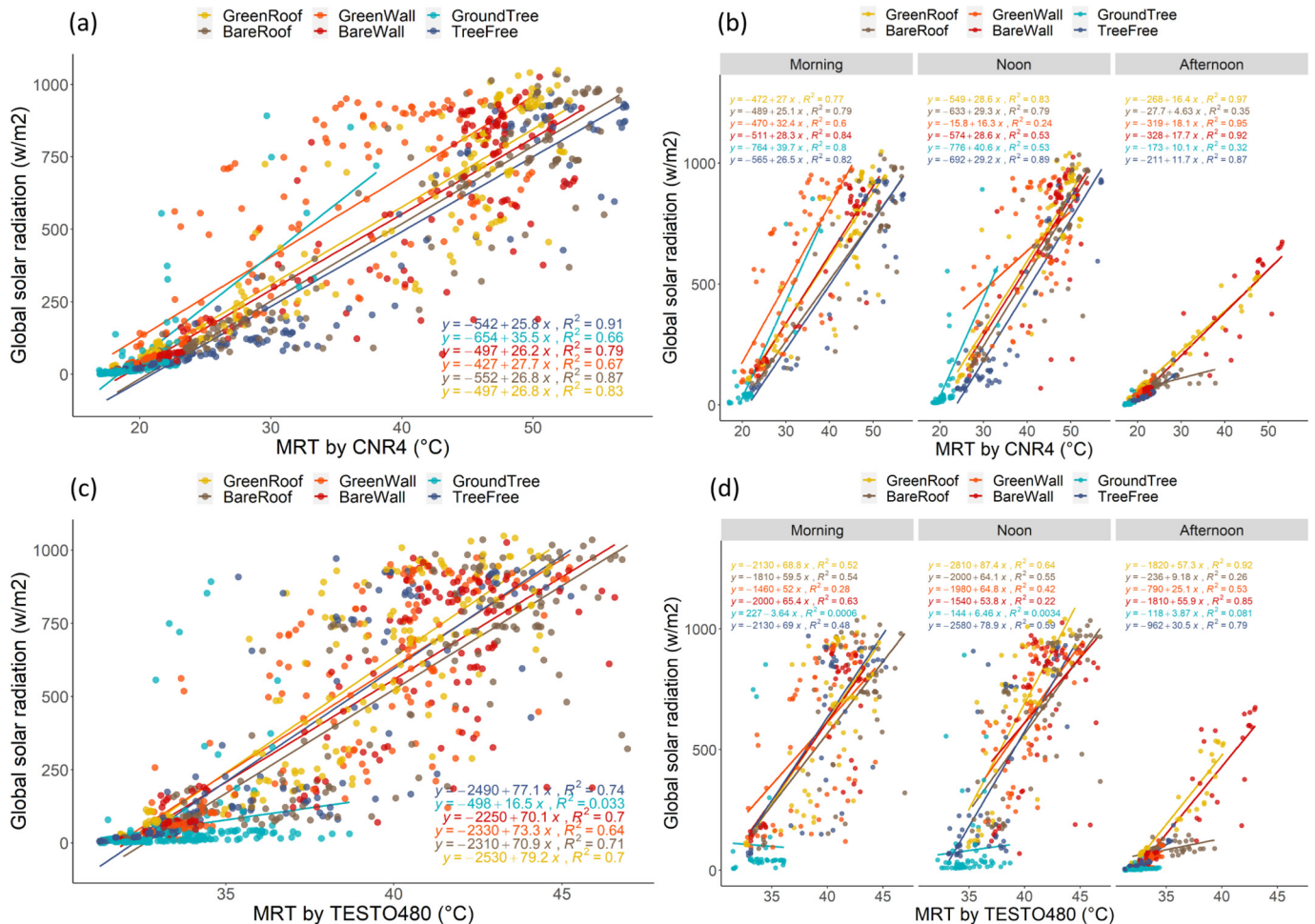


Fig. 11. Correlation between global shortwave radiation and MRT measured by two methods (a, c) daytime and (b, d) three temporal periods.

3.3. Comparing irradiant responses of two measuring methods

As previous studies compared two typical MRT measuring methods in the sites with nearly no greenery, their results and conclusions may not apply to sites with greenery covering. In this section, we presented the correlation and differences between two measuring methods regarding MRT and its contributory factors.

3.3.1. Correlation between MRT by two methods

Fig. 9 showed the correlation between MRT measured by two methods: global thermometer method (TESTO480) and six-directional method (CNR4) during daytime (Fig. 10(a)) and three temporal periods (Fig. 10(b)). In general, the ranges of MRT by CNR4 (range: 16.93–57.11 °C) was larger than that of TESTO480 (31.25–46.95 °C), and MRT by CNR4 (mean ± sd: 33.33 ± 12.55 °C) had a lower average and a higher variation than the MRT by TESTO480 (37.58 ± 4.12 °C). For different GI typologies, all six points showed positive correlations between MRTs by two methods; the correlation was especially strong for the tree-free ($R^2 = 0.89$), the bare wall ($R^2 = 0.85$), and the bare roof ($R^2 = 0.81$), but weakly correlated for the ground tree ($R^2 = 0.16$). The correlations throughout three periods were also examined because the irradiative features were different in these three periods (as discussed Section 3.2.2). In the morning, these two methods showed the highest correlation in the bare wall location ($R^2 = 0.82$) and lowest correlation in the ground tree spot ($R^2 = 0.03$), which means small differences between these two methods were found near the bare wall but larger discrepancies adjacent tree. At noon, these two methods performed similarly in the tree-free point ($R^2 = 0.78$) but showed a weak

correlation near a green wall ($R^2 = 0.22$) and the bare wall ($R^2 = 0.38$). Nearly no correlation was found near the ground tree for these two methods ($R^2 = 0.01$). During the afternoon, strong relationships were found between MRT by two methods near the bare wall, the green roof, and the tree-free location with R^2 above 0.9, while two methods responded differently for the ground tree ($R^2 = 0.18$).

3.3.2. Correlation between global shortwave radiation and MRT by two methods

To further explore whether the differences of correlation arise from shortwave radiation, correlations between MRT and global shortwave radiation (GSR) were plotted and compared in Fig. 11. For the six-directional method, MRT values in all six points showed a strong correlation with GSR, while the tree free ($R^2 = 0.91$), bare roof ($R^2 = 0.87$), and green roof ($R^2 = 0.83$) showed especially high correlation coefficients. This indicated that MRT measured by the six-directional method was largely affected by GSR. Furthermore, for temporal periods, the strong relationship was found in the morning as a high R^2 was found near the bare wall ($R^2 = 0.84$), tree-free ($R^2 = 0.82$), and ground tree ($R^2 = 0.80$). At noon, although MRT in no tree and green roof spots showed a high correlation with GSR ($R^2 = 0.89$ and 0.83 respectively), a weak coefficient of $R^2 = 0.24$ was revealed for the green wall. Similarly, in the afternoon, MRT near the spots of green roof ($R^2 = 0.97$), green wall ($R^2 = 0.95$), bare wall ($R^2 = 0.92$), and tree-free ($R^2 = 0.87$) showed high correlation with GSR, but the ground tree and the bare roof showed a moderately weak relationship with $R^2 = 0.32$ and 0.35, respectively.

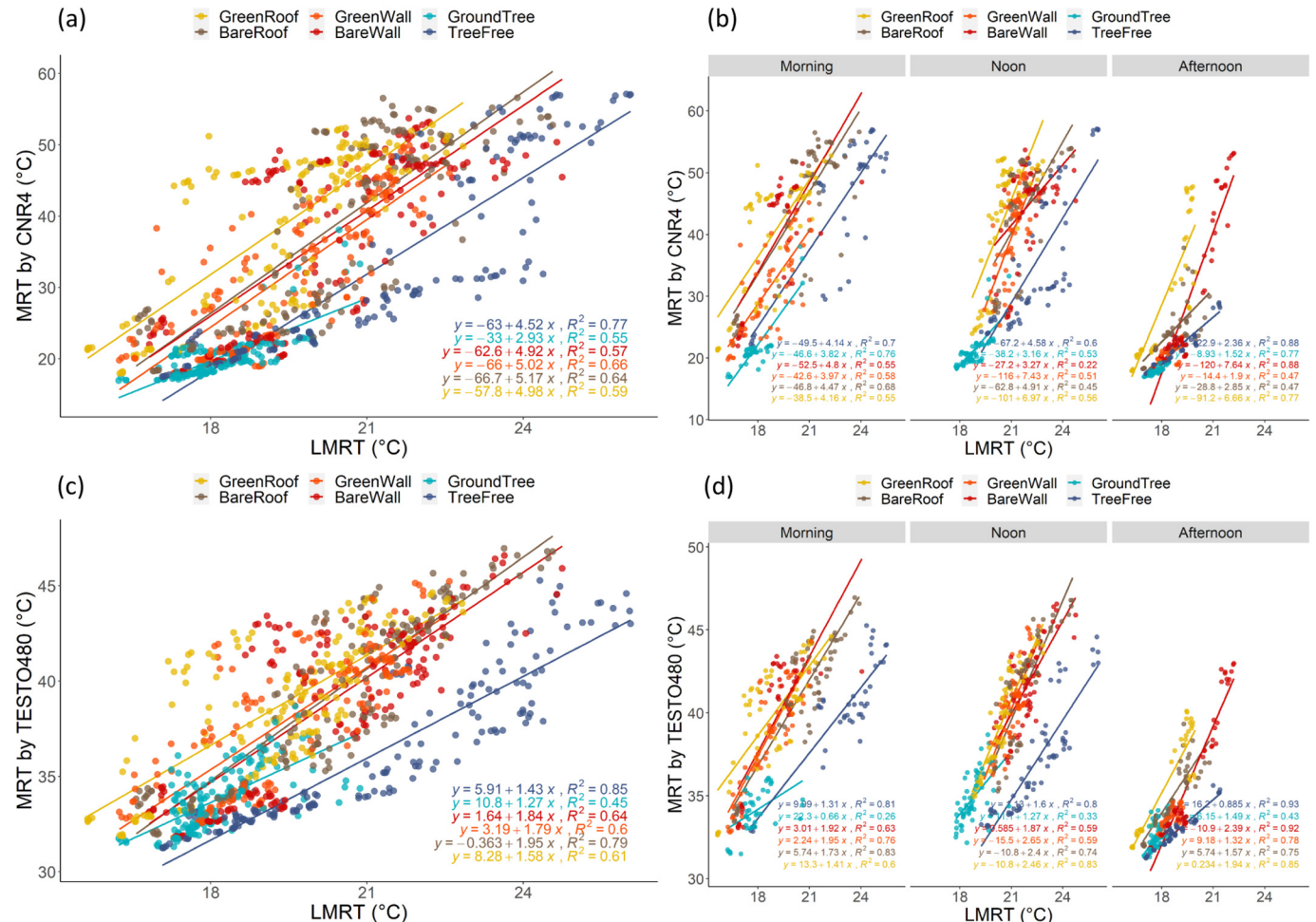


Fig. 12. Correlation between LMRT and MRT measured by two methods (a, b) LMRT vs. MRT by CNR4 (c, d) LMRT vs. MRT by TESTO480.

In terms of the globe thermometer method, during the entire daytime period, MRT and GSR were moderately correlated except at the ground tree location which showed no correlation ($R^2 = 0.03$). In deeper details for three periods, MRT near the ground tree showed no correlation with GSR throughout all three periods with $R^2 = 0.00$, 0.00, and 0.08. A weak correlation was also found for MRT near the green wall ($R^2 = 0.28$) and tree-free ($R^2 = 0.48$) in the morning, the bare wall ($R^2 = 0.22$) and the green wall ($R^2 = 0.42$) in the noon, as well as the bare roof ($R^2 = 0.26$) in the afternoon. Besides, the correlation for AT, wind speed (W_s), and global temperature (T_g) and MRT by two methods were also analyzed, which could be found in Fig. S3-1, S3-2, S3-3 in Supplementary file S3.

3.3.3. Correlation between radiant fluxes components and MRT by two methods

To investigate the different dependence of MRT on two components of MRT (LMRT for the longwave radiant part and MRT-LMRT for remaining part), the correlations between LMRT and MRT measured by two methods were shown in Fig. 12. Generally, MRT by two methods showed a positive correlation with LMRT in a moderately good coefficient of determination ($R^2 \geq 0.5$). In detail, MRT by CNR4 presented a slightly lower association with LMRT near three bare points and two GI typologies (green roof and green wall) than MRT by TESTO480, but a stronger correlation coefficient at ground tree location regardless of daytime or three temporal periods. As LMRT presents the surface temperatures of the surrounding environment (Lai et al., 2017), the results indicated MRT by CNR4 was more dependent in longwave radiant fluxes under shaded areas but less dependent in open areas, and vice versa for MRT by TESTO480.

The associations between MRT-LMRT and MRT measured by two methods were shown in Fig. 13. Apparently, MRT by CNR4 showed strong correlations with MRT-LMRT irrespective of GI typologies and temporal periods. In terms of MRT by TESTO480, low coefficients were found near the tree and the green wall although the moderate coefficients were found near bare spots and green roof. As MRT-LMRT quantified the sum of shortwave fluxes reflected and diffused by the surrounding environment, the results indicated MRT by CNR4 was highly dependent on shortwave radiant fluxes regardless of GI typologies and temporal periods, but MRT by TESTO480 only responded to shortwave fluxes comparatively in open areas. And the results of this and the last section showed the deficiency of TESTO480 under the tree shading areas.

4. Discussions and implications

4.1. Thermal and irradiant features of three GI typologies

Previous studies measured three GI typologies separately for their thermal and irradiant behaviors in different study areas, which makes comparison rather difficult and brings biased as the surrounding environmental condition and anthropogenic factors might be different (Bowler et al., 2010). Our study contributed to the limited evidence of the thermal-irradiant performance of three GI typologies within one site so that the thermal-irradiant features can be compared unbiasedly.

According to previous studies, it was observed in Hong Kong that the daytime AT difference between the green roof and bare roof on sunny days was 1.3 °C (Lee and Jim, 2020), which was slightly higher than 1.18 °C in our study for partially cloudy days. A study in Nanjing, China

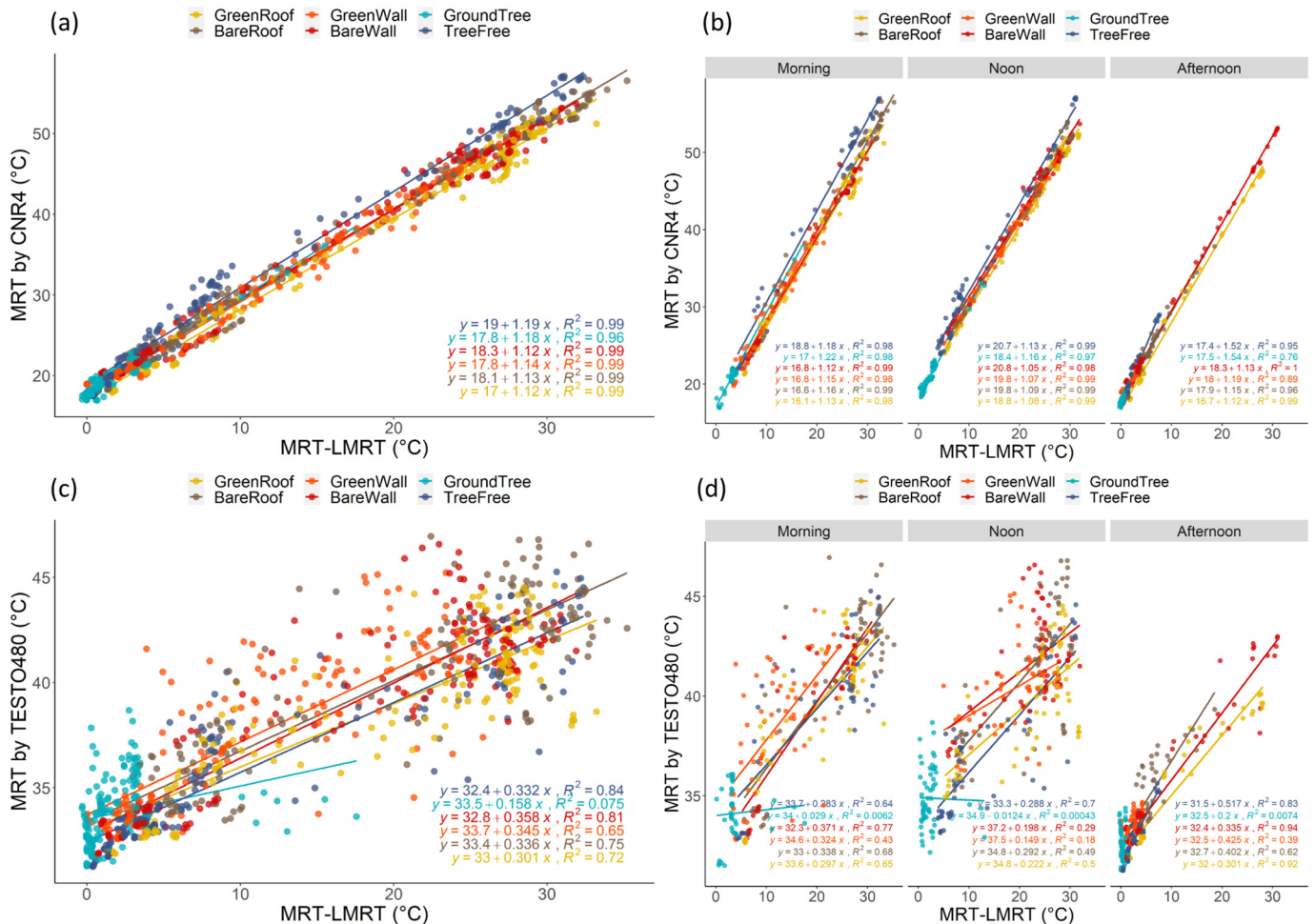


Fig. 13. Correlation between MRT-LMRT and MRT measured by two methods (a, b) MRT-LMRT vs. MRT by CNR4 (c, d) MRT-LMRT vs. MRT by TESTO480.

found a higher temperature cooling at 0.6 m height (0.23 °C) than at 1.2 m height (0.09 °C), and in sunny weather than in cloudy weather (Yin et al., 2019), while a higher cooling of 1.18 °C was found in our study at 1.5 m height under partly cloudy weather condition. Additionally, these two studies surprisingly detected a warming effect for the green roof during nighttime in Hong Kong and daytime in Nanjing, which was not found in our study. These discrepancies may be because rooftop greenery was placed in different heights above the ground (7 m in our study, 14 and 16.5 m in these two studies), also could be explained by various greenery densities, plant species, as well as variable solar intensity. Regarding green wall, MRT and AT attenuation were found within a limited distance, i.e., within 1 m. For instance, in Singapore, vertical greenery decreased MRT by up to 12.9 °C, and this attenuation was influenced by shading effects of walls (Liang et al., 2014). Our findings were in line with this study that radiant reduction was greater in the morning and afternoon periods due to building shadings. A study in Spain measured green walls in different orientations and found 0.5–2.0 °C temperature reduction and up to 7% moisture increase in the hottest months (Perez et al., 2011), which was higher than the results of this study (0.21–0.73 °C AT reduction and (–0.66)–4.71% RH increase). This difference can be attributed to the varied climate background and different greenery species. In terms of the ground tree, a study in Taiwan found tree canopy decreased AT by 0.64–2.52 °C compared with nearby unshaded areas (Lin and Lin, 2010), which was slightly higher than the results in this study (0.88–1.57 °C). In Hong Kong, researchers observed trees provided a temperature reduction of 0.4–0.6 °C averagely and by 1.7–2.6 °C maximumly in summer daytime (Cheung and Jim, 2018), which was slightly lower than the values in our study. This is partly because of the different underlying surfaces between two studies; Our study measured the combinations of both tree and grass, and this combination also showed reinforced cooling in a dry and hot climate (Shashua-Bar et al., 2011).

In respect of GI typologies comparison, our study observed similar temperature reduction by the green roof and by the ground tree (Fig. 6a), which was possible because green roof point was surrounded by other shrubs and trees and was affected by the cooling capacity of the surroundings. Besides, average daytime irradiant attenuation in MRT was achieved at 16 °C near the tree, followed by the green wall by 8 °C, but the green roof showed a minor reduction in MRT. With shading evapotranspiration process, shortwave and longwave radiations under the tree point were reduced significantly, and thus MRT under the tree was lowest for three periods (Gunawardena et al., 2017). This indicated that ground tree and vertical greenery may effectively reduce pedestrian thermal exposure (Middel and Krayenhoff, 2019; Tan et al., 2017). Although the green roof showed little contribution to the pedestrian level, it showed significant heat attenuation at the city scale (Santamouris, 2014). Therefore, future studies should explore the optimal strategies for different GI typologies and in different scales. Concerning temporal periods, our study found temperature reduction provided by GI typologies was larger before noon than in the afternoon, which was different from the findings of previous studies that the attenuation was the highest in the afternoon (Tan et al., 2017). One possible reason is the shading effects, as the EMSD building shading for six measurement points undermined the effectiveness of greenery cooling (Morakinyo et al., 2020). Further explorations should compare both effects of temporal periods and shading effects and found the main driver for GI thermal-irradiant differences.

In summary, some findings of our study were consistent with previous studies, while other findings were different. These different thermal-irradiant values should be compared and interpreted carefully, as the measurement settings, background climate, urban geometry, and greenery species and features were different and interacted complexly. This also emphasizes the necessity of our study to conduct the measurements in the same site for GI typologies, and thus the comparisons of the thermal-irradiant features are possible. Furthermore, experimental data in this study can also provide evidence to assess the reliability of the models (Francis and Jensen, 2017).

4.2. Comparison between two measuring methods for MRT

Two measuring methods for MRT estimation, namely the six-directional and globe thermometer method, have been compared and discussed in the previous studies. However, these studies mainly focused on areas with limited greenery, such as the squares and courtyard (Thorsson et al., 2007; Thorsson et al., 2006), streets with nearly no greenery (Krüger et al., 2014), and pedestrian sidewalks (Khrit et al., 2017). A study included park site but only discussed the impacts of trees on the differences of two methods (Tan et al., 2013). Our study filled the research gap of comparing the two measuring methods for their different responses towards GI typologies.

So far, a consensus has been obtained that the six-directional method is the most accurate and reliable estimation for MRT (Krüger et al., 2014; Chen et al., 2014). A study in Göteborg found small differences between these two methods with R^2 above 0.9 (Thorsson et al., 2007), which was much higher than the correlation coefficients in our study. Globe thermometer was found to overestimated MRT in Freiburg (Chen et al., 2014) and shading conditions in Göteborg (Thorsson et al., 2007); underestimated MRT in sunshine conditions in Göteborg compared with six-directional technology (Thorsson et al., 2007). Our findings were in line with this evidence that MRT by TESTO480 showed higher values under tree shading and lower values in open spaces than MRT by CNR4. Furthermore, a tropical study found larger ranges and variations for the six-directional method than the globe thermometer method (Tan et al., 2013), which corresponds to the results of our study. Another study in the tropical regions found MRT by globe thermometer overestimated MRT during the noontime but underestimated in the morning and afternoon (Khrit et al., 2017), which was not reflected in our findings. These results should be carefully compared due to the complexities of the irradiative processes in the different climate background and urban geometry context (i.e., sky view factor, greenery density), as well as different time resolution for analysis.

Contributory factors, i.e., wind speed, solar radiation, radiant fluxes components, were also explored for MRT measured by two methods in other studies. In terms of wind speed and solar radiation, some studies smoothed the rapid changes in them by using a large temporal scale, i.e., 5-min and reduced their effects in MRT discrepancies (Thorsson et al., 2007). Some studies also corrected the convection coefficients in MRT calculation equations for the globe thermometer based on wind velocity (Tan et al., 2013; Chen et al., 2014) and incoming short-wave radiation (Thorsson et al., 2007; Marino et al., 2017). In our study, however, wind speed variations showed generally no effects on MRT by both methods (Fig. S3-3), which may be due to the low wind speed at the pedestrian level in Hong Kong (Ng et al., 2011). And global shortwave radiation (GSR) showed a high correlation with MRT by CNR4 regardless of GI typologies and temporal periods. This result indicated that MRT by CNR4 was influenced by GSR significantly, which was also found in another study in Hong Kong (Lai et al., 2017). Regarding radiant fluxes, such as LMRT to represent the surface temperature in the surroundings and MRT-LMRT to represent the shortwave radiations diffused and reflected by the surroundings, a previous study in Hong Kong found a higher correlation coefficient for LMRT than for MRT-LMRT with MRT (Lai et al., 2017), which was different from the results of our study where MRT by CNR4 was dependent higher in MRT-LMRT than in LMRT. As for MRT by TESTO480, it associated significantly with T_g based on nearly perfect correlation relationships (Fig. S3-2), but less with LMRT and MRT-LMRT. Especially near ground tree location, TESTO480 showed its deficiency in MRT measuring.

In addition, previous studies applied different sizes in globe thermometer, i.e., 38 mm, 40 mm, 50 mm, and 150 mm (Cheung and Jim, 2018; Liang et al., 2014; Thorsson et al., 2007; Tan et al., 2013; Khrit et al., 2017). The sphere is smaller, the response time is shorter and equilibrium status is achieved faster. However, due to a greater effect of the convective heat change (wind speed, air temperature, etc.), the accuracy of the globe thermometer method is reduced accordingly

(Kántor et al., 2015). Besides, different sampling resolution and average ranges in time period also differed. This partly explained some differences between our study and previous studies.

To sum up, our study indicated the six-directional method showed higher sensitivity and accuracy in measuring the irradiant variations than the globe thermometer method. The Globe thermometer method cannot be used in shading environments due to its low responses towards LMRT and MRT-LMRT which should be the main components for MRT in shading areas. To overcome the shortcomings of the globe thermometer method, some studies suggested replacing black globe with grey one as the black color tends to absorb more shortwave radiation (Thorsson et al., 2007; Krüger et al., 2014), while some recommended appropriate wind adjustments (Krüger et al., 2014; Chen et al., 2014). Although the six-direction method is identified as the most accurate method to measure MRT (Krüger et al., 2014), a shortcoming was found for its relapse during noon for clear days (Kántor et al., 2014), which was not found in our study. Previous studies often discussed these two methods in different urban geometry, such as sky view factor, but seldom compared their differences regarding different GI typologies. Our study enlarges the discussion and understanding of the similarities and differences of these two methods towards different greenery typologies. Yet these two methods should undergo further exploration and improvement for suitable application situations, especially for varied contexts with different GI typologies. Once the limitations and strengths of these methods are well-known, the best selection in the method for certain research objectives and study areas could be made.

4.3. Implications for sustainable planning and design

For a local experience, HK published a comprehensive strategic plan HK2030+ to enhance livability in the high-density environment (H.K.P. Department, 2012). In this policy file, a new green index is proposed and discussed to combine ground tree, vertical greenery, and rooftop greenery. For these three GI typologies, our results suggest that they can improve pedestrian-level thermal comfort by decreasing both thermal and radiant loadings. Shading is the most significant design strategy for the outdoor thermal environment, while decreasing LMRT (surrounding surface temperature) also counts by replacing impervious surfaces with the pervious covering, especially by GI (i.e., green wall, green roof, grass cover). Based on suggested 30% greenery coverage ratios in HK's planning and design guidelines (H.K.P. Department, 2010), trees should be prioritized for GI provision and be planted based on urban geometry features accordingly (Morakinyo et al., 2020); whereas in areas without enough space to plant trees, GI strategies in optimized combinations should be considered. Our results also support the practice note 152 published by the HK government in calculating the greenery coverage ratio in both ground and skyrise locations (Greening and Development Bureau, 2013; Department, B, 2016).

Regionally, our results can also be referred to other areas and regions in the similar climate regions, such as Greater Bay Area megalopolis regions in a subtropical climate. Internationally, our study is in line with the advocate of the World Health Organization (WHO) that GI is considered as a determinant of health and well-being (World Health Organization, 2010). Strengthening GI from neighborhood to city-scale is also supported by the United Nation's (UN) (2015) Sustainable Development Goals (SDGs): SDG 3-good health and well-being and SDG11-sustainable cities and community (United Nations, 2015).

4.4. Limitations and future studies

This study has certain limitations in the measurement periods and greenery species diversity. Firstly, this study only covered diurnal periods in partially cloudy weather conditions in HK. Further measurements should include both daytime and nighttime, as well as other types of weather conditions, to get a comprehensive understanding of the thermal-irradiant performances of GI typologies (Yin et al., 2019).

Moreover, this study applied transect measurement to collect irradiant variables. If possible, stationary measurement for irradiant variables near three GI typologies should be conducted and the results could be compared with this study. Secondly, this study focused on the differences among GI typologies, thus only covered one tree species, and did not explore the differences between intensive green roof vs. extensive green roof, and green wall vs. living wall. Other trees with different features, i.e. leaf area indices (LAI), canopy densities, and shapes, etc., are worth furtherly investigating to provide more tree species selections for landscape design (Morakinyo et al., 2020; Zheng et al., 2020). Comparisons between different vertical greenery systems, green roof constructions and plant species are also necessary to study for their environmental benefits and implementations (Besir and Cuce, 2018; Zhang et al., 2020).

Several directions are worthy further investigations in the future. As this study focused on two widely used MRT measuring methods, a new method using cylindrical pyranometer was recently proposed (Brown, 2019), and worth investigating for its performance around GI typologies. Besides, the comparisons between relative humidity and absolute humidity for their differences and representativeness in humidity level, especially near GI typologies, are also valuable. Lastly, further studies should explore optimized strategies in different GI combinations for local climate and urban built environment contexts.

5. Conclusion

To ensure the cross-comparisons among GI typologies in the similar climate background and urban geometry settings, this study firstly conducted the field measurements on the thermal-irradiant variables at six points (three GI typologies) within one site in a subtropical climate city. Secondly it compared the thermal-irradiant performance of three GI typologies in different temporal periods with descriptive statistics and ANOVA analysis. Given previous studies only compared the globe thermometer and the six-directional methods in greenery free sites, our study compared the radiant features measured by these two methods for their different responses towards GI typologies; the contributory factors for the discrepancies between them were investigated.

The important findings can be drawn as below in three aspects:

- For GI typologies, the ground tree showed the highest reduction and the lowest fluctuations in thermal-irradiant features, followed by the green roof and the green wall. Shading effects from the surrounding building had impacts on the thermal-irradiant performance of GI typologies.
- For temporal periods, the morning session (9:30–12:00) had the highest AT reduction, RH increment, and MRT variations among the three GI typologies, followed by the noon (12:01–15:00) and afternoon periods (15:01–17:25).
- For two MRT measuring methods, the six-directional method performed higher sensitivity towards the radiation variations, and therefore had higher ranges and different responses on three GI typologies; the globe thermometer tended to overestimate MRT with low global solar radiation (GSR) and underestimate MRT with high GSR.

The present study provides a comprehensive understanding of the thermal-irradiant performance of three GI typologies, which may assist landscape designers and policymakers for climate responsive design. Also, this study underscores the necessity to select the MRT measuring method carefully according to certain built environments and research targets, especially avoiding using the globe thermometer method in the shaded sites, such as under the tree canopy.

CRedit authorship contribution statement

Wanlu Ouyang: Conceptualization, Methodology, Investigation, Formal analysis, Visualization, Writing – original draft, Writing –

review & editing. **Tobi Eniolu Morakinyo:** Methodology, Investigation, Writing – review & editing. **Chao Ren:** Supervision, Writing – review & editing. **Sheng Liu:** Investigation, Writing – review & editing. **Edward Ng:** Supervision, Writing – review & editing, Funding acquisition.

Declaration of competing interest

The authors declare no conflict of interest with the present submission and with the content of this paper.

Appendix A

Table A1
Descriptive statistics for the thermal difference on four selected measurement days.

Date (YYYY-MM-DD)	Index	Greenery type	Max	Min	Mean	Std
2019-09-07	ΔAT (°C)	Green roof	0.06	-2.72	-1.23	0.54
		Green wall	-0.09	-1.64	-0.73	0.28
		Ground tree	-0.02	-4.44	-1.57	1.10
	ΔRH (%)	Green roof	11.11	-3.15	0.42	2.30
		Green wall	6.96	-1.46	2.27	1.94
		Ground tree	15.50	-0.34	6.27	4.63
2019-09-09	ΔAT (°C)	Green roof	0.17	-2.65	-1.01	0.53
		Green wall	0.48	-1.16	-0.21	0.26
		Ground tree	-0.25	-2.46	-0.88	0.49
	ΔRH (%)	Green roof	6.73	-0.55	3.31	1.43
		Green wall	5.99	-4.68	-0.66	2.41
		Ground tree	12.92	-0.18	4.46	3.63
2019-09-11	ΔAT (°C)	Green roof	0.53	-3.13	-1.38	0.90
		Green wall	0.00	-1.40	-0.56	0.28
		Ground tree	0.00	-4.18	-1.17	0.75
	ΔRH (%)	Green roof	6.89	-5.50	2.00	2.40
		Green wall	4.98	-2.73	0.54	1.43
		Ground tree	16.23	-0.27	3.78	4.17
2019-09-12	ΔAT (°C)	Green roof	0.46	-3.14	-1.10	0.72
		Green wall	0.12	-1.95	-0.66	0.38
		Ground tree	-0.25	-3.93	-1.32	0.85
	ΔRH (%)	Green roof	10.19	-5.92	1.51	3.84
		Green wall	11.13	0.21	4.71	2.59
		Ground tree	15.50	-0.29	6.09	5.02

Table A2
Descriptive statistics for the radiant temperature on four selected measurement days (unit: [°C]).

Date (YYYY-MM-DD)	Radiant temperature		Green roof	Bare roof	Green wall	Bare wall	Ground tree	Tree free	
2019-09-07	MRT	Max	49.76	53.46	46.65	51.47	36.09	57.01	
		Min	20.90	23.00	18.92	19.55	17.84	21.17	
		Mean	34.15	39.01	30.06	34.27	20.76	33.26	
		Sd.	9.91	11.62	8.42	10.99	3.59	11.66	
		LMRT	Max	22.85	23.42	21.53	23.42	20.60	24.70
			Min	17.39	18.60	17.92	18.10	17.38	19.13
	Mean		19.52	21.13	19.56	20.30	18.57	22.25	
	MRT-LMRT	Sd.	1.27	1.34	1.10	1.37	0.87	1.93	
		Max	27.60	32.47	25.82	30.88	15.51	32.37	
		Min	3.50	3.03	0.01	0.93	0.03	2.01	
	2019-09-09	MRT	Mean	14.63	17.88	10.50	13.97	2.19	11.01
			Sd.	9.18	10.67	7.71	10.22	2.96	10.15
Max			52.36	50.37	49.91	53.17	30.06	50.91	
Min			17.92	18.26	17.92	18.10	16.93	17.48	
Mean			35.22	34.36	32.59	35.27	19.46	29.65	
Sd.			12.81	12.56	11.48	13.71	2.99	12.04	
LMRT		Max	21.58	22.62	21.82	22.60	19.79	24.13	
		Min	15.64	16.57	16.25	16.83	16.24	17.08	
		Mean	18.49	19.30	19.09	19.76	17.74	19.81	
		Sd.	1.99	2.13	1.90	2.25	0.82	2.18	
		MRT-LMRT	Max	33.23	28.93	28.10	30.97	11.05	27.09
			Min	1.66	1.34	0.62	0.74	0.02	0.39
Mean	16.74		15.05	13.50	15.51	1.72	9.84		
2019-09-11	MRT	Sd.	10.99	10.76	9.89	11.70	2.44	10.11	
		Max	50.60	55.03	48.37	53.70	38.05	54.40	
		Min	20.09	21.28	19.82	20.24	17.19	18.90	
		Mean	43.68	43.60	33.03	40.28	20.45	32.52	

Table A2 (continued)

Date (YYYY-MM-DD)	Radiant temperature		Green roof	Bare roof	Green wall	Bare wall	Ground tree	Tree free	
2019-09-12	LMRT	Sd.	9.12	11.88	9.10	11.37	4.37	12.82	
		Max	21.81	22.28	21.47	22.33	20.87	24.23	
		Min	16.52	17.61	17.69	17.95	17.27	17.52	
		Mean	19.53	20.56	19.58	20.28	18.01	20.75	
	MRT-LMRT	Sd.	1.58	1.46	1.40	1.47	0.80	2.34	
		Max	29.81	32.97	26.90	31.90	17.58	31.06	
		Min	3.53	3.65	1.98	2.27	0.01	1.38	
		Mean	24.15	23.04	13.45	20.00	2.44	11.77	
	MRT	Sd.	7.94	10.61	7.88	10.22	3.67	10.67	
		Max	52.78	56.60	46.00	50.51	22.25	57.11	
		Min	21.25	23.52	20.01	21.51	17.51	19.67	
		Mean	40.38	41.32	31.62	39.61	19.66	35.69	
	LMRT	Sd.	10.06	11.45	9.65	10.70	1.69	14.73	
		Max	22.82	24.56	22.58	24.75	19.37	26.06	
		Min	16.79	18.13	16.54	18.20	17.25	18.42	
		Mean	19.74	21.22	19.65	20.91	18.23	22.02	
	MRT-LMRT	Sd.	1.76	1.97	1.74	1.99	0.68	2.79	
		Max	30.52	35.21	24.27	28.03	3.98	31.65	
		Min	4.40	4.20	1.87	3.22	0.04	1.25	
		Mean	20.64	20.10	11.97	18.71	1.43	13.67	
			Sd.	8.73	9.90	8.22	9.44	1.43	12.14

Appendix B. Supplementary data

Supplementary data to this article can be found online at <https://doi.org/10.1016/j.scitotenv.2020.144635>.

References

- de Abreu-Harbach, L.V., Labaki, L.C., Matzarakis, A., 2015. Effect of tree planting design and tree species on human thermal comfort in the tropics. *Landsc. Urban Plan.* 138, 99–109.
- Alexandri, E., Jones, P., 2008. Temperature decreases in an urban canyon due to green walls and green roofs in diverse climates. *Build. Environ.* 43 (4), 480–493.
- ASHRAE, H., 2001. *ASHRAE Fundamentals Handbook*. American Society of Heating Refrigeration and Air-Conditioning Engineers, Atlanta GA.
- B. Department, 2016. *Sustainable Building Design Guidelines (SBD Guidelines) (PNAP) APP-152*.
- Bartasaghi Koc, C., Osmond, P., Peters, A., 2018. Evaluating the cooling effects of green infrastructure: a systematic review of methods, indicators and data sources. *Sol. Energy* 166, 486–508.
- Bastin, J.-F., et al., 2019. Understanding climate change from a global analysis of city analogues. *PLoS One* 14(7).
- Besir, A.B., Cuce, E., 2018. Green roofs and facades: a comprehensive review. *Renew. Sust. Energ. Rev.* 82, 915–939.
- Bowler, D.E., et al., 2010. Urban greening to cool towns and cities: a systematic review of the empirical evidence. *Landsc. Urban Plan.* 97 (3), 147–155.
- Brown, R.D., 2019. Correcting the error in measuring radiation received by a person: introducing cylindrical radiometers. *Sensors* 19 (23), 5085.
- Chen, L., et al., 2012. Sky view factor analysis of street canyons and its implications for daytime intra-urban air temperature differentials in high-rise, high-density urban areas of Hong Kong: a GIS-based simulation approach. *Int. J. Climatol.* 32 (1), 121–136.
- Chen, Y.-C., Lin, T.-P., Matzarakis, A., 2014. Comparison of mean radiant temperature from field experiment and modelling: a case study in Freiburg, Germany. *Theor. Appl. Climatol.* 118 (3), 535–551.
- Cheung, P.K., Jim, C.Y., 2018. Comparing the cooling effects of a tree and a concrete shelter using PET and UTCL. *Build. Environ.* 130, 49–61.
- Coutts, A.M., et al., 2013. Assessing practical measures to reduce urban heat: green and cool roofs. *Build. Environ.* 70, 266–276.
- D'Orazio, M., Di Perna, C., Di Giuseppe, E., 2012. Green roof yearly performance: a case study in a highly insulated building under temperate climate. *Energy Build.* 55, 439–451.
- Francis, L.F.M., Jensen, M.B., 2017. Benefits of green roofs: a systematic review of the evidence for three ecosystem services. *Urban For. Urban Green.* 28, 167–176.
- Greening, L.A.T.M.S., Development Bureau, 2013. *Skyrise Greenery - Pictorial Guide to Plant Resources for Skyrise Greenery in Hong Kong*.
- Gunawardena, K.R., Wells, M.J., Kershaw, T., 2017. Utilising green and bluespace to mitigate urban heat island intensity. *Sci. Total Environ.* 584–585, 1040–1055.
- H.K.P. Department, 2010. *Hong Kong Planning Standards and Guidelines*.
- H.K.P. Department, 2012. *Hong Kong 2030: Planning Vision and Strategy*. Strategic Planning Section, Hong Kong Planning Department Hong Kong.
- Heating, A.S.o., Refrigerating, and A.-C. Engineers, 1985. *ASHRAE Handbook, 1985 Fundamentals: An Instrument of Service Prepared for the Profession Containing Technical Information*. The Society.
- Hong Kong Observatory, The year's weather – 2019 <https://www.weather.gov.hk/en/wxinfo/pastwx/2019/ywx2019.htm> [Accessed on 12th Mar 2020]. 2020a.
- Hong Kong Observatory, Climate projections for Hong Kong: temperature https://www.weather.gov.hk/en/climate_change/proj_hk_temp.htm [Accessed on 12th Mar 2020b].
- IPCC, 2014a. *Climate Change 2014–Impacts, Adaptation and Vulnerability: Regional Aspects*. Cambridge University Press.
- IPCC, 2014b. In: Team, Core Writing, Pachauri, R.K., Meyer, L.A. (Eds.), *Climate Change 2014: Synthesis Report. Contribution of Working Groups I, II and III to the Fifth Assessment Report of the Intergovernmental Panel on Climate Change*. IPCC, Geneva, Switzerland 151 pp.
- Kántor, N., Lin, T.-P., Matzarakis, A., 2014. Daytime relapse of the mean radiant temperature based on the six-directional method under unobstructed solar radiation. *Int. J. Biometeorol.* 58 (7), 1615–1625.
- Kántor, N., Kovács, A., Lin, T.-P., 2015. Looking for simple correction functions between the mean radiant temperature from the “standard black globe” and the “six-directional” techniques in Taiwan. *Theor. Appl. Climatol.* 121 (1), 99–111.
- Khrit, N., et al. Assessing the accuracy of globe thermometer method in predicting outdoor mean radiant temperature under Malaysia tropical microclimate. In *E3S Web of Conferences*. 2017. EDP Sciences.
- Krayenhoff, E.S., et al., 2018. Diurnal interaction between urban expansion, climate change and adaptation in US cities. *Nat. Clim. Chang.* 8 (12), 1097–1103.
- Krüger, E., Minella, F., Matzarakis, A., 2014. Comparison of different methods of estimating the mean radiant temperature in outdoor thermal comfort studies. *Int. J. Biometeorol.* 58 (8), 1727–1737.
- Kuehn, L.A., Stubbs, R.A., Weaver, R.S., 1970. Theory of the globe thermometer. *J. Appl. Physiol.* 29 (5), 750–757.
- Lai, A., Maing, M., Ng, E., 2017. Observational studies of mean radiant temperature across different outdoor spaces under shaded conditions in densely built environment. *Build. Environ.* 114, 397–409.
- Lai, D., et al., 2019. A review of mitigating strategies to improve the thermal environment and thermal comfort in urban outdoor spaces. *Sci. Total Environ.* 661, 337–353.
- Lee, L.S., Jim, C.Y., 2019. Urban woodland on intensive green roof improved outdoor thermal comfort in subtropical summer. *Int. J. Biometeorol.* 63 (7), 895–909.
- Lee, L.S., Jim, C.Y., 2020. Thermal-irradiance behaviours of subtropical intensive green roof in winter and landscape-soil design implications. *Energy Build.* 209, 109692.
- Li, X., et al., 2016. Environmental inequities in terms of different types of urban greenery in Hartford, Connecticut. *Urban Forest. Urban Green.* 18, 163–172.
- Liang, T.C., Hien, W.N., Jusuf, S.K., 2014. Effects of vertical greenery on mean radiant temperature in the tropical urban environment. *Landsc. Urban Plan.* 127, 52–64.
- Lin, B.-S., Lin, Y.-J., 2010. Cooling effect of shade trees with different characteristics in a subtropical urban park. *HortScience* 45 (1), 83–86.
- Manoli, G., et al., 2019. Magnitude of urban heat islands largely explained by climate and population. *Nature* 573 (7772), 55–60.
- Marino, C., et al., 2017. The effect of the short wave radiation and its reflected components on the mean radiant temperature: modelling and preliminary experimental results. *J. Build. Eng.* 9, 42–51.
- Mazzali, U., et al., 2013. Experimental investigation on the energy performance of living walls in a temperate climate. *Build. Environ.* 64, 57–66.
- Middel, A., Krayenhoff, E.S., 2019. Micrometeorological determinants of pedestrian thermal exposure during record-breaking heat in Tempe, Arizona: introducing the MarTy observational platform. *Sci. Total Environ.* 687, 137–151.
- Morakinyo, T.E., et al., 2017. A study on the impact of shadow-cast and tree species on incanyon and neighborhood's thermal comfort. *Build. Environ.* 115, 1–17.

- Morakinyo, T.E., et al., 2020. Right tree, right place (urban canyon): tree species selection approach for optimum urban heat mitigation – development and evaluation. *Sci. Total Environ.* 719, 137461.
- Ng, E., et al., 2011. Improving the wind environment in high-density cities by understanding urban morphology and surface roughness: a study in Hong Kong. *Landsc. Urban Plan.* 101 (1), 59–74.
- Nyuk Hien, W., Yok, T. Puay, Yu, C., 2007. Study of thermal performance of extensive rooftop greenery systems in the tropical climate. *Build. Environ.* 42 (1), 25–54.
- Oke, T.R., et al., 2017. *Urban Climates*. Cambridge University Press.
- Ong, B.L., 2003. Green plot ratio: an ecological measure for architecture and urban planning. *Landsc. Urban Plan.* 63 (4), 197–211.
- Ouldboukhitine, S.-E., Belarbi, R., Sailor, D.J., 2014. Experimental and numerical investigation of urban street canyons to evaluate the impact of green roof inside and outside buildings. *Appl. Energy* 114, 273–282.
- Perez, G., et al., 2011. Green vertical systems for buildings as passive systems for energy savings. *Appl. Energy* 88 (12), 4854–4859.
- Pérez, G., et al., 2014. Vertical Greenery Systems (VGS) for energy saving in buildings: a review. *Renew. Sust. Energ. Rev.* 39, 139–165.
- R Core Team, 2020. R: A Language and Environment for Statistical Computing. R Foundation for Statistical Computing, Vienna, Austria URL <https://www.R-project.org/>.
- Raji, B., Tenpierik, M.J., van den Dobbelsteen, A., 2015. The impact of greening systems on building energy performance: a literature review. *Renew. Sust. Energ. Rev.* 45, 610–623.
- Ren, C., Ng, E.Y.Y., Katzschner, L., 2011. Urban climatic map studies: a review. *Int. J. Climatol.* 31 (15), 2213–2233.
- Ritchie, H., Roser, M., 2018. *Urbanization*. Our World in Data.
- Roth, M., 2007. Review of urban climate research in (sub) tropical regions. *Int. J. Climatol.* 27 (14), 1859–1873.
- Santamouris, M., 2014. Cooling the cities – a review of reflective and green roof mitigation technologies to fight heat island and improve comfort in urban environments. *Sol. Energy* 103, 682–703.
- Shashua-Bar, L., Hoffman, M.E., 2000. Vegetation as a climatic component in the design of an urban street: an empirical model for predicting the cooling effect of urban green areas with trees. *Energy Build.* 31 (3), 221–235.
- Shashua-Bar, L., Pearlmutter, D., Erell, E., 2011. The influence of trees and grass on outdoor thermal comfort in a hot-arid environment. *Int. J. Climatol.* 31 (10), 1498–1506.
- Solcerova, A., et al., 2017. Do green roofs cool the air? *Build. Environ.* 111, 249–255.
- Susorova, I., Azimi, P., Stephens, B., 2014. The effects of climbing vegetation on the local microclimate, thermal performance, and air infiltration of four building facade orientations. *Build. Environ.* 76, 113–124.
- Tan, C.L., Wong, N.H., Jusuf, S.K., 2013. Outdoor mean radiant temperature estimation in the tropical urban environment. *Build. Environ.* 64, 118–129.
- Tan, Z., Lau, K.K.-L., Ng, E., 2016. Urban tree design approaches for mitigating daytime urban heat island effects in a high-density urban environment. *Energy Build.* 114, 265–274.
- Tan, Z., Lau, K.K.-L., Ng, E., 2017. Planning strategies for roadside tree planting and outdoor comfort enhancement in subtropical high-density urban areas. *Build. Environ.* 120, 93–109.
- Thorsson, S., et al., 2006. Measurements of mean radiant temperature in different urban structures. 6th International Conference on Urban Climate. Urban Climate Group, Department of Geosciences, Göteborg University, Sweden.
- Thorsson, S., et al., 2007. Different methods for estimating the mean radiant temperature in an outdoor urban setting. *Int. J. Climatol.* 27 (14), 1983–1993.
- Toudert, F.A., 2005. Dependence of Outdoor Thermal Comfort on Street Design in Hot and Dry Climate. Meteorologisches Institut der Albert-Ludwigs-Universität.
- United Nations, 2015. *Transforming our World: The 2030 Agenda for Sustainable Development*. United Nations, Department of Economic and Social Affairs, New York.
- Wong, N.H., et al., 2003. Investigation of thermal benefits of rooftop garden in the tropical environment. *Build. Environ.* 38 (2), 261–270.
- Wong, N.H., et al., 2010. Thermal evaluation of vertical greenery systems for building walls. *Build. Environ.* 45 (3), 663–672.
- World Health Organization, 2010. *Health 2020: A European Policy Framework Supporting Action across Government and Society for Health and Well-being*.
- Yang, J., Bou-Zeid, E., 2019. Scale dependence of the benefits and efficiency of green and cool roofs. *Landsc. Urban Plan.* 185, 127–140.
- Yin, H., et al., 2017. Cooling effect of direct green façades during hot summer days: an observational study in Nanjing, China using TIR and 3DPC data. *Build. Environ.* 116, 195–206.
- Yin, H., et al., 2019. Investigation of extensive green roof outdoor spatio-temporal thermal performance during summer in a subtropical monsoon climate. *Sci. Total Environ.* 696, 133976.
- Yoshida, A., et al., 2015. Evaluation of effect of tree canopy on thermal environment, thermal sensation, and mental state. *Urban Clim.* 14, 240–250.
- Zhang, G., He, B.-J., Dewancker, B.J., 2020. The maintenance of prefabricated green roofs for preserving cooling performance: a field measurement in the subtropical city of Hangzhou, China. *Sustain. Cities Soc.* 61, 102314.
- Zheng, S., et al., 2020. Modeling of shade creation and radiation modification by four tree species in hot and humid areas: case study of Guangzhou, China. *Urban Forest. Urban Green.* 47, 126545.